EUROPEAN ORGANIZATION FOR NUCLEAR RESEARCH (CERN)

CERN-EP-20XX-ZZZ
LHCb-PAPER-2022-037
October 19, 2022

A study of *CP* violation in the decays $B^{\pm} \to [K^+K^-\pi^+\pi^-]_D h^{\pm}$ $(h = K, \pi)$ and $B^{\pm} \to [\pi^+\pi^-\pi^+\pi^-]_D h^{\pm}$

LHCb collaboration[†]

Abstract

The first study of *CP* violation in the decay mode $B^{\pm} \to [K^+K^-\pi^+\pi^-]_D h^{\pm}$ $(h = K, \pi)$ is presented, exploiting a data sample of proton-proton collisions collected by the LHCb experiment that corresponds to an integrated luminosity of $9\,\text{fb}^{-1}$. The analysis is performed in bins of phase space, which are optimised for sensitivity to local *CP* asymmetries. *CP*-violating observables that are sensitive to the angle γ of the Unitarity Triangle are determined. The analysis requires external information on charm-decay parameters, which are currently taken from an amplitude model, but can be updated in future when direct measurements become available. Measurements are also performed of phase-space integrated observables for $B^{\pm} \to [K^+K^-\pi^+\pi^-]_D h^{\pm}$ and $B^{\pm} \to [\pi^+\pi^-\pi^+\pi^-]_D h^{\pm}$.

To be submitted to Eur. Phys. J. C

[†]Authors are listed at the end of this paper.

1 Introduction

The Standard Model (SM) description of charge-parity (CP) violation can be tested by measuring the lengths and angles of the Unitary Triangle, which is a geometrical representation of the Cabibbo–Kobayashi–Maskawa quark-mixing matrix [1, 2]. In particular, the CP-violating phase $\gamma \equiv \arg(-V_{ud}V_{ub}^*/V_{cd}V_{cb}^*)$ is the only angle that can be measured at tree level, with negligible theoretical uncertainties [3]. Therefore, it makes an excellent SM benchmark that can be compared with other indirect measurements of γ that are more likely to be affected by New Physics.

A powerful channel for the measurement of γ is $B^\pm \to DK^\pm$, which proceeds through both a favoured $b \to c\bar{u}s$ and a suppressed $b \to u\bar{c}s$ transition. Interference occurs when the D meson, which is a superposition of D^0 and $\overline{D}^0$, decays to a final state common to both of these flavour eigenstates. The interference effects are sensitive to γ, which can in general be determined from measurements of the appropriate CP asymmetries and related observables. This strategy has been pursued for a wide range of D final states at LHCb [4–8] and other b-physics experiments [9–11]. CP-violating effects also occur in the process $B^\pm \to D\pi^\pm$ through the interference of $b \to c\bar{u}d$ and $b \to u\bar{c}d$ transitions, but these are in general significantly lower in magnitude.

An interesting class of D final states are self-conjugate multi-body D decays. Since the strong-phase difference between the D^0 and $\overline{D}^0 \to K^+K^-\pi^+\pi^-$ decays varies across the multi-dimensional phase space of the charm-meson decay, the sensitivity to γ is diluted when considering the decay inclusively. However, by performing measurements in suitably chosen localised regions of phase space, the dilution effects can be minimised and the sensitivity to γ enhanced [12–15].

The channel $D \to K^+K^-\pi^+\pi^-$ has been proposed as a promising decay mode for measuring γ [16]. It has a rich resonance structure and contains only charged particles in the final state, which is advantageous for experiments at a hadron collider. The availability of a detailed amplitude model for this process [17] opens up the possibility of identifying those regions of phase space that have high sensitivity to γ, which then can be probed in an analysis of $B^\pm \to DK^\pm$ decays. The interpretation of the CP asymmetries and other observables in these regions requires knowledge of the strong-phase difference of the charm-meson decay. This knowledge can be obtained from the same amplitude model used to guide the measurements, but it is preferable to take the information from direct determinations made by experiments at charm threshold, as this approach ensures the determination of γ has no dependence on model assumptions. An analogous study has recently been performed using the decay mode $D \to K^\pm\pi^\mp\pi^\pm\pi^\mp$ [18].

This paper presents a first study of CP violation in $B^\pm \to [K^+K^-\pi^+\pi^-]_D h^\pm$ decays, with $h = K, \pi$. The analysis exploits proton-proton (pp) collision data collected by LHCb in Runs 1 and 2 of the LHC corresponding to 9 fb^{-1} of integrated luminosity. The study is performed in localised regions of phase space, defined with guidance from the amplitude model presented in Ref. [17], and the measurements are used to extract a value of γ, using model predictions for the strong-phase variation in the charm-meson decay. In addition, first measurements of the global CP asymmetries are made for this decay and updated global measurements for the mode $B^\pm \to [\pi^+\pi^-\pi^+\pi^-]_D h^\pm$, which are also interpreted in terms of γ and the underlying physics parameters.

2 Analysis strategy

This analysis follows the formalism described in Ref. [6]. The $B^- \to [K^+K^-\pi^+\pi^-]_D K^-$ decay can proceed via the favoured $B^- \to D^0 K^-$ amplitude, or via the suppressed $B^- \to \overline{D}^0 K^-$ amplitude. The overall amplitude of this decay is a coherent sum of the two decay paths,

$$\mathcal{A}_{B^-}(\Phi) = \mathcal{A}_{B^-}^{D^0K^-}\Big(\mathcal{A}_{D^0}(\Phi) + r_B^{DK}\exp\big(i(\delta_B^{DK}-\gamma)\big)\mathcal{A}_{\overline{D}^0}(\Phi)\Big), \tag{1}$$

where $\mathcal{A}_{B^-}^{D^0K^-}$ is the amplitude of the favoured $B^- \to D^0K^-$ decay, $\mathcal{A}_{D^0}$ ($\mathcal{A}_{\overline{D}^0}$) is the amplitude of the D^0 ($\overline{D}^0$) decay, r_B^{DK} is the magnitude of the ratio of the B-decay amplitudes, δ_B^{DK} is the strong-phase difference of the amplitudes and γ is the weak-phase. Here Φ labels the position in the five-dimensional phase space of the decay $D^0 \to K^+K^-\pi^+\pi^-$. The corresponding expression for the B^+ decay is obtained by making the substitutions $\gamma \to -\gamma$ and $\mathcal{A}_{D^0} \to \mathcal{A}_{\overline{D}^0}$. Assuming here and in the subsequent discussion that *CP* violation in the D-meson system can be neglected, which is a good assumption at the current level of experimental sensitivity [19], $\mathcal{A}_{\overline{D}^0}(\Phi) = \mathcal{A}_{D^0}(\bar{\Phi})$, where the *CP*-conjugated phase space position $\bar{\Phi}$ is obtained by swapping the charges and momentum directions of the D-decay products.

The D-decay phase space is split into $2\times\mathcal{N}$ bins, labelled from $i=-\mathcal{N}$ to $i=\mathcal{N}$, excluding zero. Bin $-i$ is related to bin $+i$ by a *CP* transformation. The choice of binning is described in Sec. 3. The expected yield of B^- decays in bin i is obtained by integrating Eq. (1), and the corresponding expression for B^+ decays, over the phase space Φ_i that belongs to that particular bin. Defining the *CP*-violating observables

$$x_\pm^{DK} = r_B^{DK}\cos(\delta_B^{DK}\pm\gamma), \quad y_\pm^{DK} = r_B^{DK}\sin(\delta_B^{DK}\pm\gamma), \tag{2}$$

the yields $N_i^\pm$ of $B^\pm$ candidates in bin i are given by

$$N_{+i}^+ = h_{B^+}^{DK}\Big(F_{-i} + \big((x_+^{DK})^2+(y_+^{DK})^2\big)F_{+i} + 2\sqrt{F_{+i}F_{-i}}\big(x_+^{DK}c_i - y_+^{DK}s_i\big)\Big), \tag{3}$$

$$N_{-i}^- = h_{B^-}^{DK}\Big(F_{-i} + \big((x_-^{DK})^2+(y_-^{DK})^2\big)F_{+i} + 2\sqrt{F_{+i}F_{-i}}\big(x_-^{DK}c_i - y_-^{DK}s_i\big)\Big), \tag{4}$$

where $h_{B^\pm}^{DK}$ are normalisation constants. Since $h_{B^+}^{DK}$ and $h_{B^-}^{DK}$ are independent fit parameters, the binned measurement is insensitive to the $B^\pm$ production asymmetry and charge asymmetry in the detection efficiency of the kaon that accompanies the D meson.

Equations (3) and (4) are sensitive to γ through the interference terms, and the magnitude of the interference is determined by the size of $r_B^{DK} \approx 0.1$ [20]. The parameters F_i are defined as

$$F_i = \frac{\int_i \mathrm{d}\Phi\,\eta(\Phi)|\mathcal{A}_{D^0}|^2}{\int \mathrm{d}\Phi\,\eta(\Phi)|\mathcal{A}_{D^0}|^2}, \tag{5}$$

which are interpreted as the fractional yield of D^0 decays in bin i measured by experiment. The function $\eta(\Phi)$ accounts for the experimental acceptance, which in general depends on the location of the decay in phase space. The strong-phase information is encoded in the parameters c_i and s_i, where

$$c_i = \frac{\int_i \mathrm{d}\Phi|\mathcal{A}_{D^0}||\mathcal{A}_{\overline{D}^0}|\cos(\Delta\delta_D)}{\sqrt{\int_i \mathrm{d}\Phi|\mathcal{A}_{D^0}|^2\int_i \mathrm{d}\Phi|\mathcal{A}_{\overline{D}^0}|^2}}, \tag{6}$$

which is the amplitude-averaged cosine of the strong-phase difference $\Delta\delta_D = \delta_D(\Phi) - \delta_D(\bar{\Phi})$ of the D decay. The expression for the amplitude-averaged sine of the strong-phase difference s_i is analogous. It follows that $\bar{F}_i = F_{-i}$, $c_{-i} = c_i$ and $s_{-i} = -s_i$, where $\bar{F}_i$ are the corresponding $\overline{D}^0$ fractional bin yields. The values of c_i and s_i are currently taken from an amplitude model [17]. In the future it is expected that direct measurements of c_i and s_i will become available from a sample of correlated $D\overline{D}$ decays collected by the BESIII experiment at charm threshold [21]. The anticipated size of this sample leads to the choice of $\mathcal{N} = 8$ for the number of bins.

Analogous expressions to Eqs. 2, 3 and 4 can be written for the decay mode $B^\pm \to D\pi^\pm$, with the DK superscripts replaced by $D\pi$. Since the decay topology is identical to that of $B^\pm \to DK^\pm$, the phase-space acceptance $\eta(\Phi)$ is expected to be very similar. Thus the F_i parameters can be considered as common between $B^\pm \to D\pi^\pm$ and $B^\pm \to DK^\pm$ decays. The mode $B^\pm \to D\pi^\pm$ has a branching fraction that is an order of magnitude larger than that of $B^\pm \to DK^\pm$, but the interference effects, governed by the parameter $r_B^{D\pi} \approx 0.005$ [20], are much smaller. Therefore, this decay has a significantly lower sensitivity to γ, but is a suitable mode for determining the F_i parameters. By including $B^\pm \to D\pi^\pm$ as a signal mode, the F_i can be treated as free parameters in the analysis, thus avoiding the need to know the form of the $\eta(\Phi)$ acceptance function.

From the definition in Eq. (5), it follows that $\sum_i F_i = 1$. Therefore, only $2\mathcal{N} - 1$ of the $2\mathcal{N}$ F_i parameters are independent. To accommodate this constraint in the analysis, the F_i parameters are fitted with the alternative parameterisation

$$F_i = \begin{cases} R_i, & i = -N \\ R_i \prod_{j<i}(1 - R_j), & -N < i < +N \\ \prod_{j<i}(1 - R_j), & i = +N. \end{cases} \tag{7}$$

Measuring the yields of $B^\pm$ decays in each bin of phase space allows the eight *CP*-violating observables $x_\pm^{DK}$, $y_\pm^{DK}$, $x_\pm^{D\pi}$ and $y_\pm^{D\pi}$ to be determined. These *CP*-violating observables can be interpreted in terms of the five underlying physics parameters γ, δ_B^{DK}, r_B^{DK}, $\delta_B^{D\pi}$ and $r_B^{D\pi}$.

Studies performed with pseudoexperiments demonstrate that a fit where all eight *CP*-violating observables are free parameters is unstable for $r_B^{D\pi} < 0.03$, due to large correlations between the $B^\pm \to D\pi^\pm$ *CP*-violating observables and the F_i parameters [6]. Since γ is a common parameter between the $B^\pm \to DK^\pm$ and $B^\pm \to D\pi^\pm$ analyses, the *CP*-violating observables for the $B^\pm \to D\pi^\pm$ mode can be re-parameterised as

$$x_\xi^{D\pi} = \Re\big(\xi^{D\pi}\big), \quad y_\xi^{D\pi} = \Im\big(\xi^{D\pi}\big), \quad \xi^{D\pi} = \frac{r_B^{D\pi}}{r_B^{DK}} \exp\Big(i\big(\delta_B^{D\pi} - \delta_B^{DK}\big)\Big). \tag{8}$$

In summary, a measurement of the bin yields of $B^\pm \to [K^+K^-\pi^+\pi^-]_D h^\pm$ decays in bins of phase space, allows the six *CP*-violating observables $x_\pm^{DK}$, $y_\pm^{DK}$, $x_\xi^{D\pi}$ and $y_\xi^{D\pi}$ to be determined, along with the experiment-specific parameters F_i, expressed in terms of R_i, and the four normalisation parameters $h_{B^\pm}^{Dh}$.

Additionally, γ can be constrained further by measuring the phase-space inclusive *CP*-violating observables [22, 23]. In the case of $D \to K^+K^-\pi^+\pi^-$ these are the charge asymmetries

$$A_h^{KK\pi\pi} = \frac{\Gamma(B^- \to Dh^-) - \Gamma(B^+ \to Dh^+)}{\Gamma(B^- \to Dh^-) + \Gamma(B^+ \to Dh^+)}, \tag{9}$$

for $h = \pi$, K, and the double ratio

$$R_{CP}^{KK\pi\pi} = \frac{R_{KK\pi\pi}}{R_{K\pi\pi\pi}}, \quad R_f = \frac{\Gamma(B^- \to [f]_D K^-) + \Gamma(B^+ \to [f]_D K^+)}{\Gamma(B^- \to [f]_D \pi^-) + \Gamma(B^+ \to [f]_D \pi^+)}, \tag{10}$$

where in the case of $R_{K\pi\pi\pi}$ the kaon from the D-meson decay has the same charge as the pion or kaon from the B-meson decay. The value of $R_{K\pi\pi\pi}$ can be determined from the results presented in Ref. [18]. By integrating Eqs. (3) and (4) over all bins i, it can be shown that these phase-space inclusive CP-violating observables may be expressed in terms of the underlying physics parameters,

$$A_h^{KK\pi\pi} = \frac{2 r_B^{Dh} \kappa \sin(\delta_B^{Dh}) \sin(\gamma)}{1 + (r_B^{Dh})^2 + 2 r_B^{Dh} \kappa \cos(\delta_B^{Dh}) \cos(\gamma)}, \tag{11}$$

$$R_{CP}^{KK\pi\pi} = 1 + (r_B^{DK})^2 + 2 r_B^{DK} \kappa \cos(\delta_B^{DK}) \cos(\gamma), \tag{12}$$

where $\kappa = 2F_+^{KK\pi\pi} - 1$ is the dilution factor when integrating over all of phase space, with $F_+^{KK\pi\pi}$ being the CP-even fraction of the decay. In Eqs. (11) and (12), the small effects of charm mixing have been neglected, but these may readily be included [24]. Analogous observables $A_h^{\pi\pi\pi\pi}$ and $R_{CP}^{\pi\pi\pi\pi}$ exist for the decay $D \to \pi^+\pi^-\pi^+\pi^-$.

3 Binning scheme

In the $B^\pm \to DK^\pm$, $D \to K^0_S h^+ h^-$ ($h = \pi, K$) analysis presented in Ref. [6], an optimal binning scheme, that can be visualised in a two-dimensional Dalitz plot, is used to maximise the sensitivity to γ. The binning scheme for $D^0 \to K^+K^-\pi^+\pi^-$ is defined analogously, but cannot be easily visualised, as the phase space of four-body decays is five-dimensional.

When defining a binning scheme for the decay $D \to K^+K^-\pi^+\pi^-$, there are two main requirements. Firstly, it should minimise the dilution of the strong phases when averaged over each bin. Secondly, it should maximise the interference effects and thus the sensitivity to γ. The scheme is constructed with the guidance of the amplitude model presented in Ref. [17].

The position of a D decay in phase space is specified by the four-momenta of the decay products. These four-momenta allow the corresponding decay amplitudes $\mathcal{A}_{D^0}$ and $\mathcal{A}_{\overline{D}^0}$ of the D^0 and $\overline{D}^0$ decays, respectively, to be determined from the amplitude model. From the D^0 and $\overline{D}^0$ decay amplitudes, two convenient parameters,

$$\Delta\delta_D \equiv \arg\left(\frac{\mathcal{A}_{D^0}}{\mathcal{A}_{\overline{D}^0}}\right), \quad r_D \equiv \left|\frac{\mathcal{A}_{D^0}}{\mathcal{A}_{\overline{D}^0}}\right|, \tag{13}$$

are defined. These are the strong-phase difference and the magnitude of the ratio between the D^0 and $\overline{D}^0$ amplitudes according to the model, respectively. Effectively, by considering $\Delta\delta_D$ and r_D as parameters, each D decay in the five-dimensional phase space is projected onto a two-dimensional surface, where a binning scheme can be defined.

The binning is first performed in the $\Delta\delta_D$ coordinate, which spans the range $-\pi \leq \Delta\delta_D < +\pi$ and is divided into $\mathcal{N}$ bins with boundaries that are symmetric around $\Delta\delta_D = 0$. Assigning a decay to such a bin ensures it is grouped with other decays with a similar strong-phase difference, which minimises the dilution in sensitivity to γ. Bin i is then

divided into two, with labels i and $-i$ according to the value of r_D, giving $2 \times \mathcal{N}$ bins in total. This division is performed in a manner to enhance the difference between F_{+i} and F_{-i}, which maximises the magnitude of the interference terms in Eqs. (3) and (4). Candidates with $\ln r_D < 0$ (> 0) are assigned to bin $i > 0$ (< 0), and the bin numbering starts at $i = \mathcal{N}$ ($i = 1$) near $\Delta\delta_D = -\pi$, with decreasing (increasing) bin numbers.

Following the procedure described in Ref. [25], the binning scheme is optimised by adjusting the bin boundaries in $\Delta\delta_D$ to maximise the Q-value, defined as $Q^2 = (Q_+^2 + Q_-^2)/2$, where

$$Q_\pm^2 = 1 - \Big(1 - \sum_i \frac{F_i F_{-i}\big(1 - c_i^2 - s_i^2\big)}{N_i^\pm}\Big)\Big(\sum_i F_i\Big)^{-1}. \tag{14}$$

Here $N_i^\pm$, the $B^\pm \to DK^\pm$ decay yields in bin i, as predicted by Eqs. (3) and (4), are calculated with the normalisation coefficients $h_{B^\pm}$ set to unity. The parameters $Q_\pm$ give the statistical sensitivity of $x_\pm$ and $y_\pm$ from a binned fit, divided by that of an unbinned fit. With an infinite number of bins, $Q \to 1$. This metric neglects any perturbation to the sensitivity that may arise from the presence of background events.

Only even values of $\mathcal{N}$ are considered and the bin boundaries at $\Delta\delta_D = 0$ and $\pm\pi$ are fixed. Then each pair of bin boundaries on either side of $\Delta\delta_D = 0$ are adjusted until the Q-value is maximal. In each iteration F_i, c_i and s_i are calculated from the amplitude model using Eqs. (5) and (6), assuming a uniform acceptance. The five-dimensional integral over phase space is performed with Monte Carlo integration. Large samples of D-decays are generated for the integration, such that the uncertainty due to the finite sample size is negligible. The values of $N_i^\pm$ are determined from Eqs. (3) and (4), and take as input $\gamma = 75^\circ$, $\delta_B^{DK} = 130^\circ$ and $r_B^{DK} = 0.1$, which lie close to the known values of these parameters [20]. Note, however, that Q has a very weak dependence on the values of the phases assumed in these expressions, and so this choice does not bias the analysis.

Figure 1a shows the binning scheme resulting from this procedure for 2×8 bins, and the values of c_i and s_i predicted by the amplitude model are shown in Table 1, along with the predicted values of F_i and the fractional bin volume V_i. In the calculation, the region of phase space where the invariant mass of the $\pi^+\pi^-$ lies close to the K^0_S mass is excluded. This requirement, which removes around 5% of signal decays, is imposed to match a selection requirement to remove background that is described in Sec. 5.

The binning scheme shown in Fig. 1a has $Q = 0.90$, which indicates that 10% of the statistical sensitivity is lost through the binning of phase space. A procedure for assigning bin numbers for this scheme according to the four-momenta of the D decay is provided in Ref. [26]. An alternative optimised binning scheme with $\mathcal{N} = 4$ is presented in Appendix A.

The determination of the *CP*-violating parameters requires as input the values of c_i and s_i in each bin. Although the bins have been defined using the amplitude model, it will be possible to use direct measurements of these parameters made at charm threshold, when they become available. The choice of binning scheme does not bias the determination of the *CP*-violating parameters, even if the direct measurements were to indicate that the amplitude model gives an imperfect description of the strong-phase variation. In this case, there would be a reduction in statistical sensitivity compared to current expectations, but the result obtained for γ would have no model-dependent uncertainty.

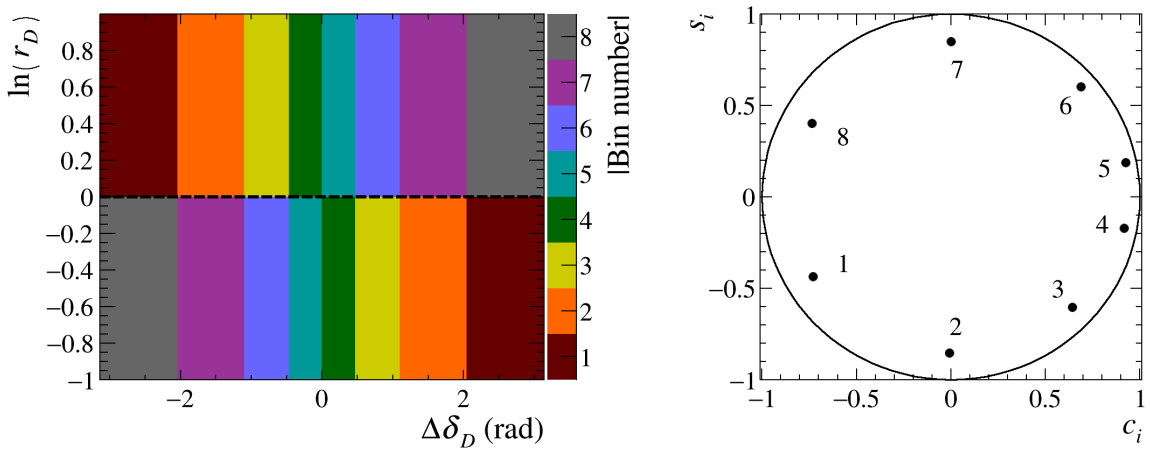

(a) 2×8 binning scheme.

(b) c_i and s_i

Figure 1: The optimised 2×8 binning scheme in $\Delta\delta_D$-ln(r_D) space and the associated c_i and s_i parameters calculated using the amplitude model.

Table 1: c_i, s_i, F_i and V_i for the optimised 2×8 binning scheme, as calculated from the amplitude model.

Bin number	c_i	s_i	F_i	F_{-i}	V_i	V_{-i}
1	−0.7317	−0.4343	0.0157	0.0495	0.0555	0.0555
2	−0.0076	−0.8528	0.0185	0.0644	0.0645	0.0645
3	0.6406	−0.6056	0.0295	0.1024	0.0753	0.0754
4	0.9151	−0.1728	0.0687	0.1466	0.0654	0.0655
5	0.9247	0.1887	0.0815	0.1646	0.0742	0.0742
6	0.6853	0.6021	0.0398	0.0973	0.0665	0.0664
7	−0.0032	0.8490	0.0143	0.0488	0.0510	0.0510
8	−0.7368	0.4041	0.0132	0.0451	0.0475	0.0476

4 The LHCb detector and data set

The analysis uses data collected by the LHCb experiment in pp collisions at $\sqrt{s} = 7\,\text{TeV}$, 8 TeV and 13 TeV. The data sets correspond to integrated luminosities of $1\,\text{fb}^{-1}$, $2\,\text{fb}^{-1}$ and $6\,\text{fb}^{-1}$, respectively.

The LHCb detector [27, 28] is a single-arm forward spectrometer covering the pseudorapidity range $2 < \eta < 5$, designed for the study of particles containing b or c quarks. The detector includes a high-precision tracking system consisting of a silicon-strip vertex detector surrounding the pp interaction region, a large-area silicon-strip detector located upstream of a dipole magnet with a bending power of about 4 Tm, and three stations of silicon-strip detectors and straw drift tubes placed downstream of the magnet. The tracking system provides a measurement of the momentum, p, of charged particles with a relative uncertainty that varies from 0.5% at low momentum to 1.0% at 200 GeV/c. The minimum distance of a track to a primary pp collision vertex (PV), the impact parameter (IP), is measured with a resolution of $(15 + 29/p_{\text{T}})\,\mu\text{m}$, where p_{T} is

the component of the momentum transverse to the beam, in GeV/c. Different types of charged hadrons are distinguished using information from two ring-imaging Cherenkov detectors. Photons, electrons and hadrons are identified by a calorimeter system consisting of scintillating-pad and preshower detectors, an electromagnetic and a hadronic calorimeter. Muons are identified by a system composed of alternating layers of iron and multiwire proportional chambers. The online event selection is performed by a trigger, which consists of a hardware stage, based on information from the calorimeter and muon systems, followed by a software stage, which applies a full event reconstruction.

Simulation is required to model the effects of the detector acceptance, and for the study of possible background processes. In the simulation, pp collisions are generated using Pythia [29] with a specific LHCb configuration [30]. Decays of unstable particles are described by EvtGen [31], in which final-state radiation is generated using Photos [32]. The $D^0 \to K^+K^-\pi^+\pi^-$ decay is simulated using the amplitude model from Ref. [17]. The interaction of the generated particles with the detector, and its response, are implemented using the Geant4 toolkit [33] as described in Ref. [34]. The underlying pp interaction is reused multiple times, with an independently generated signal decay for each [35].

5 Candidate selection

A $B^\pm$ candidate is reconstructed by combining five charged tracks. Four of the charged tracks are required to have an invariant mass within $25\,\text{MeV}/c^2$ of the D^0 mass. This requirement, which corresponds to around two and a half times the resolution of the mass peak, removes processes that have either a missing or misidentified particle. Candidates where the opening angle between any pair of tracks from the D-decay products is smaller than 0.03° are discarded, as these are likely to be hits from a single charged particle that is duplicated in the reconstruction.

To suppress charmless background, which arises from $B^\pm$ meson decays where there is no intermediate charm meson, the distance between the D and $B^\pm$ decay vertices is required to be greater than twice its resolution for the binned measurement. This criterion eliminates 95% of this category of decays. In the phase-space inclusive measurement, which is found to be more sensitive to this source of contamination, the decay distance requirement is tightened to four times its resolution, suppressing the background by a further order of magnitude.

Separation of $B^\pm \to DK^\pm$ and $B^\pm \to D\pi^\pm$ decays is achieved by imposing mutually exclusive particle identification (PID) requirements on the companion track, which is the $K^\pm$ or $\pi^\pm$ meson of the $B^\pm \to Dh^\pm$ decay. Companion tracks that have associated activity in the muon detector are removed; this requirement reduces background from semi-leptonic b-hadron decays involving a muon which is misidentified as a companion kaon or pion. Background from semi-leptonic b-decays involving an electron is found to be negligible.

Background from D decays where a $\pi^+\pi^-$ pair originates from a K^0_S meson is suppressed by excluding regions containing $\pi^+\pi^-$ pairs with invariant mass inside the interval $[477, 507]\,\text{MeV}/c^2$ from the binning scheme. Additionally, PID requirements are imposed on the kaon from the D candidate with opposite sign to the companion track. This selection requirement suppresses $D \to K^\mp\pi^\pm\pi^-\pi^+\pi^0$ background where the π^0 meson is not reconstructed and the kaon is misidentified.

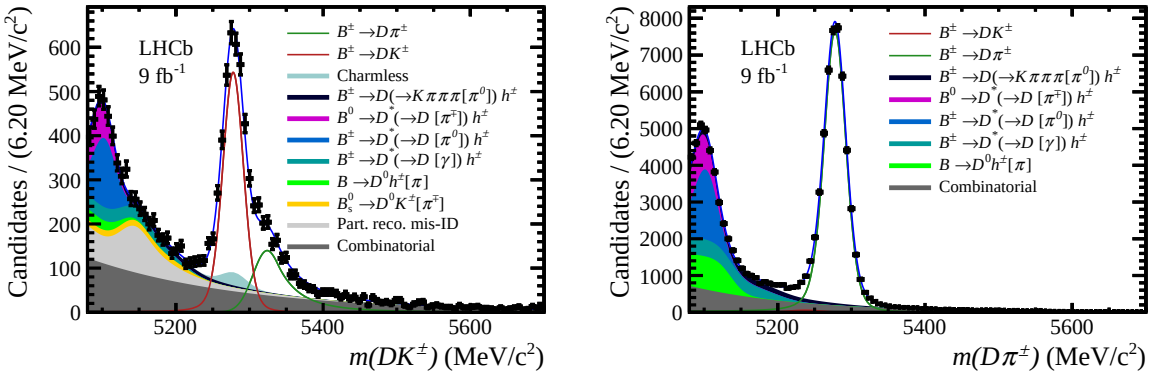

Figure 2: Invariant-mass distributions for the (left) $B^\pm \to DK^\pm$ selection and (right) $B^\pm \to D\pi^\pm$ selection, with $D \to K^+K^-\pi^+\pi^-$. The square brackets in the legend denote particles that are not reconstructed.

Combinatorial background is suppressed using a boosted decision tree (BDT) algorithm [36, 37] implemented in the TMVA toolkit [38]. Simulated signal events are used as a signal training sample, while candidates in the far upper sideband of the $B^\pm$ sideband between 5800-7000 MeV/c^2 form a background training sample. The input variables of the BDT include the momenta and IPs of the $B^\pm$, D and companion-track candidates. The parameters are described in detail in Ref. [39]. The optimal working point of the BDT is determined by performing pseudoexperiments to determine the cut value that provides the best sensitivity to γ. Candidates with a BDT score below this cut value are discarded.

To improve the resolution of the momenta of the D-decay products and the invariant mass of the $B^\pm$ candidate, a kinematic fit is performed in which the $B^\pm$ candidate is required to originate from the PV with the smallest impact parameter, by constraining the reconstructed momentum to point back to it, and the D meson is constrained to its known mass [40].

6 Invariant-mass fits

An unbinned, extended maximum-likelihood fit is performed simultaneously to the invariant-mass spectrum of the $B^\pm \to [K^-K^+\pi^+\pi^-]_D h^\pm$ and $B^\pm \to [\pi^-\pi^+\pi^+\pi^-]_D h^\pm$ candidates in the range from 5080 MeV/c^2 to 5700 MeV/c^2. The fit is first performed on the $B^\pm \to DK^\pm$ and $B^\pm \to D\pi^\pm$ candidates, integrated over all phase-space bins, which is referred to as the global fit. The global fit is used to determine the parameters of the functions that describe the signal and background distributions in invariant mass. The $B^\pm \to [K^-K^+\pi^+\pi^-]_D h^\pm$ invariant-mass distributions are shown in Fig. 2.

The yield of $B^\pm \to D\pi^\pm$ is floated separately for the two D decays, while the yield of $B^\pm \to DK^\pm$ is parameterised as a ratio relative to the $B^\pm \to D\pi^\pm$ yield. This ratio is a common fit parameter for the two D decays, as are the parameters that describe the signal shape.

The peak at around 5280 MeV/c^2 corresponds to correctly reconstructed $B^\pm \to [K^+K^-\pi^+\pi^-]_D h^\pm$ candidates. The signal invariant-mass shape is parameterised as

$$f_{\rm signal}(m|m_B,\sigma,\alpha_L,\alpha_R,\beta,k) = k \times f_{\rm MG}(m|m_B,\sigma,\alpha_L,\alpha_R,\beta) + (1-k) \times f_{\rm G}(m|m_B,\sigma),$$

where $f_{\rm G}$ is a Gaussian function and $f_{\rm MG}$ is a modified Gaussian function,

$$f_{\rm MG}(m|m_B,\sigma,\alpha_L,\alpha_R,\beta) \propto \begin{cases} \exp\left(-\frac{\Delta m^2(1+\beta\Delta m^2)}{2\sigma^2+\alpha_L\Delta m^2}\right), & \Delta m = m - m_B < 0, \\ \exp\left(-\frac{\Delta m^2(1+\beta\Delta m^2)}{2\sigma^2+\alpha_R\Delta m^2}\right), & \Delta m = m - m_B > 0. \end{cases}$$

The function $f_{\rm MG}$ has approximately gaussian behaviour when $\Delta m^2 \ll \sigma^2/\alpha_{L,R}$ or $\Delta m^2 \gg \beta^{-1}$, but it has tails that model the effect of the experimental resolution of LHCb. The tail parameters $\alpha_{L,R}$ and β, and the fraction k, are determined in a fit to simulated events, but the peak position m_B and the width σ are determined in the fit to data. The mass m_B is common between $B^\pm \to DK^\pm$ and $B^\pm \to D\pi^\pm$, but σ is different because the $B^\pm \to DK^\pm$ width is narrower due to the lower energy release in the decay.

At masses above the $B^\pm \to DK^\pm$ peak there is a non-negligible contribution from $B^\pm \to D\pi^\pm$ decays where the companion is misidentified as a kaon. The rate of this cross-feed background is fixed from the relative PID efficiencies, which are determined in calibration data, reweighted to match the momentum and pseudorapidity distributions of the companion track of the signal. The exact shape is determined using a data-driven method by swapping the mass hypothesis of the companion track in the $B^\pm \to D\pi^\pm$ peak. Similarly, the shape of $B^\pm \to DK^\pm$ misidentified as $B^\pm \to D\pi^\pm$ is also accounted for, but the impact of this background is minimal due to the smaller branching fraction.

The candidates with masses below that of the signal peak are background from B-meson decays where a neutral particle or charged pion is not reconstructed. This partially reconstructed background is described using a model developed in Ref. [6]. In this analysis the parameterisation of partially reconstructed background is taken from Ref. [6], with the exception of the contamination from $B^0_s \to \overline{D}{}^0 K^-\pi^+$ and $\overline{B}{}^0_s \to D^0 K^+\pi^-$ decays with a missing pion. The total yield of this latter background is fixed in the fit according to the results in Ref. [7].

Additionally, the decay $D \to K^+K^-\pi^+\pi^-$ is also contaminated by $D \to K^\mp\pi^\pm\pi^-\pi^+\pi^0$ decays, where a charged pion is misidentified as a kaon and the neutral pion is not reconstructed. This background is present below the signal peak, but it has a large tail towards the upper end of the invariant mass spectrum of the $B^\pm$ candidates as well. The shape of this background is fixed using a simulation sample, while the yield is a free parameter. The ratio between this background and signal is common between the $B^\pm \to DK^\pm$ and $B^\pm \to D\pi^\pm$ modes.

The contamination of charmless decays in the $D \to K^+K^-\pi^+\pi^-$ mode is also different from Ref. [6]. In particular, the $B^\pm \to [K^+K^-\pi^+\pi^-]_D K^\pm$ sample has a significant contribution from the mode $B^\pm \to K^+K^-\pi^+\pi^-K^\pm$. Both the magnitude and invariant-mass shape of this contribution is fixed in the invariant-mass fit from studies of the lower sideband of the invariant D mass. Study of the lower sideband of the D-meson invariant-mass distribution indicates that there is no significant contamination from charmless decays in the $B^\pm \to D\pi^\pm$ selection.

The signal yields, obtained from the invariant-mass fit, integrated over all phase space bins, are given in Table 2. Yields and uncertainties are appropriately scaled from the full fit region. The uncertainties on the $B^\pm \to DK^\pm$ yields are reduced due to the common ratio determined from both the $D \to K^+K^-\pi^+\pi^-$ and $D \to \pi^+\pi^-\pi^+\pi^-$ decay modes.

After the global invariant-mass fit, a second fit is performed where the $B^\pm \to DK^\pm$ and $B^\pm \to D\pi^\pm$ candidates are split by charge and sorted into bins of phase space, which makes

Table 2: Yields of $B^\pm \to DK^\pm$ and $B^\pm \to D\pi^\pm$ candidates, partially reconstructed background, combinatorial background and charmless background in the region $m_B \in [5249, 5309]\,\text{MeV}/c^2$, where $D \to K^+K^-\pi^+\pi^-$ and $D \to \pi^+\pi^-\pi^+\pi^-$. The partially reconstructed background for the $D \to K^+K^-\pi^+\pi^-$ mode also includes $D \to K^\mp\pi^\pm\pi^-\pi^+\pi^0$ decays. Additionally, in the $B^\pm \to DK^\pm$ sample the partially reconstructed background includes real partially reconstructed background, misidentified partially reconstructed background and background from B_s^0 decays. The uncertainties are statistical only.

		Reconstructed as:	
D decay	Component	$B^\pm \to DK^\pm$	$B^\pm \to D\pi^\pm$
$D \to K^+K^-\pi^+\pi^-$	$B^\pm \to DK^\pm$	3026 ± 38	142 ± 2
	$B^\pm \to D\pi^\pm$	240 ± 1	44349 ± 218
	Partially reconstructed bkg	131 ± 13	607 ± 168
	Combinatorial bkg	460 ± 23	1820 ± 193
	Charmless bkg	189 (fixed)	N/A
$D \to \pi^+\pi^-\pi^+\pi^-$	$B^\pm \to DK^\pm$	8676 ± 105	386 ± 5
	$B^\pm \to D\pi^\pm$	676 ± 2	126322 ± 386
	Partially reconstructed bkg	256 ± 2	81 ± 4
	Combinatorial bkg	1344 ± 27	4172 ± 90
	Charmless bkg	688 (fixed)	N/A

a total of $2 \times 2 \times 16 = 64$ categories. The lower fit boundary is increased to $5150\,\text{MeV}/c^2$ to remove most of the partially reconstructed background. The shape parameters and relative yields of the different background components are fixed from the global fit. The signal yields in each bin are parameterised in terms of the *CP*-violating observables, which are free parameters in the fit. The F_i parameters are also free parameters, while the strong-phase parameters c_i and s_i are fixed from the LHCb amplitude model.

In each bin, the yield of combinatorial background and partially reconstructed background are free parameters, with the exception of the $B_s^0 \to \overline{D}^0 K^-\pi^+$ contamination (and charge-conjugated case), which is treated separately because the charm meson has the opposite flavour to the signal decay and the other partially reconstructed backgrounds. In B^- (B^+) decays, the fractional bin yield of the B_s^0 ($\overline{B}_s^0$) background is therefore set equal to F_{-i} (F_i).

The distribution of the charmless background between phase-space bins is determined from the lower D-mass sideband. The distribution of $D \to K^\mp\pi^\pm\pi^-\pi^+\pi^0$ decays between phase space bins is assumed to be proportional to the bin volume, given in Table 1, since studies of simulation samples show that these decays are approximately uniform in the $D \to K^+K^-\pi^+\pi^-$ phase space.

Fit biases and instabilities in the fit are studied by performing pseudoexperiments. The pull distributions of $x_\pm^{DK}$ and $y_\pm^{DK}$ are found to be consistent with a Gaussian distribution of width 1, and a mean consistent with 0. The results for $x_\xi^{D\pi}$ and $y_\xi^{D\pi}$ show biases of up to 7% and widths that show up to 17% overcoverage. Corrections are applied to the measured values in the data to account for these effects.

The fitted *CP*-violating observables are listed in Table 3 and plotted in Fig. 3, along with the likelihood contours, which only include statistical uncertainties. The lengths of

Table 3: *CP*-violating observables of the binned measurement, multiplied by 10^2. The first uncertainty is statistical, the second is systematic, and the third is associated with the model dependence of the strong-phase parameters.

CP-violating observable	Fit result
x_-^{DK}	$7.9 \pm 2.9 \pm 0.4 \pm 0.4$
y_-^{DK}	$-3.3 \pm 3.4 \pm 0.4 \pm 3.6$
x_+^{DK}	$-12.5 \pm 2.5 \pm 0.3 \pm 1.7$
y_+^{DK}	$-4.2 \pm 3.1 \pm 0.3 \pm 1.3$
$x_\xi^{D\pi}$	$-3.1 \pm 3.5 \pm 0.7 \pm 0.1$
$y_\xi^{D\pi}$	$-1.7 \pm 4.7 \pm 0.6 \pm 1.1$

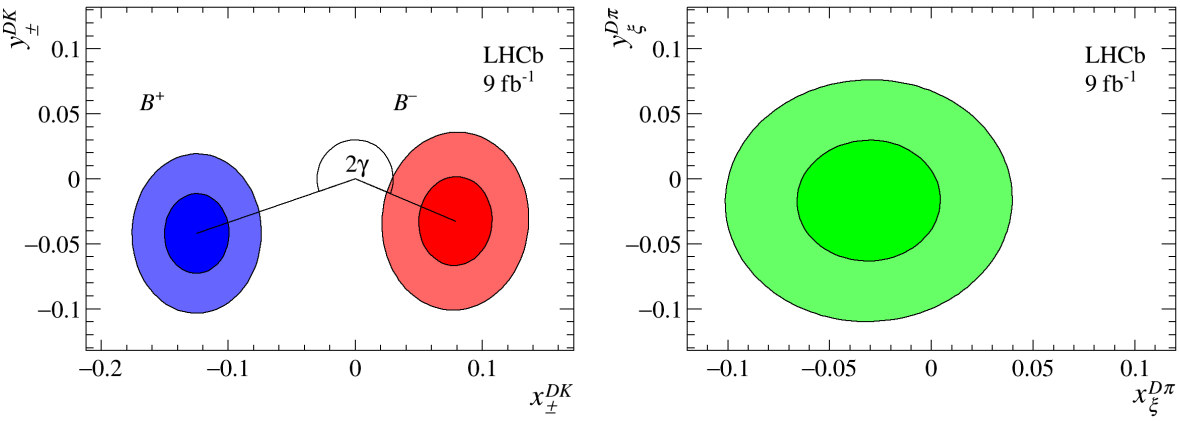

(a) $B^\pm \to DK^\pm$. (b) $B^\pm \to D\pi^\pm$.

Figure 3: Graphical representation of the *CP*-violating observables. The 1σ and 2σ contours, which represent the statistical uncertainties, are also shown. On the left, the blue (red) contours belong to the *CP*-violating observables of the $B^+ \to DK^+$ ($B^- \to DK^-$) decay, while on the right the green contours represent the $(x_\xi^{D\pi}, y_\xi^{D\pi})$ observables of the $B^\pm \to D\pi^\pm$ decay mode.

the two vectors from the origin to $(x_\pm^{DK}, y_\pm^{DK})$ determine r_B^{DK}, while the angle between them is equal to 2γ. In the absence of *CP* violation, the two vectors would be identical. The vector from the origin to $(x_\xi^{D\pi}, y_\xi^{D\pi})$ indicates the relative size and angle between r_B and δ_B of the $B^\pm \to D\pi^\pm$ and $B^\pm \to DK^\pm$ decays. Since this contour overlaps with the origin, the sensitivity to *CP* violation is much smaller in the $B^\pm \to D\pi^\pm$ mode.

The *CP*-violation effects can be illustrated directly by considering the asymmetries in each bin. This information is obtained from an alternative fit where the signal yields, instead of the *CP*-violating observables, are determined. The bin asymmetries, $(N_i^- - N_{-i}^+)/(N_i^- + N_{-i}^+)$, calculated from these yields are shown in Fig. 4. The bin yields are normalised separately for B^- and B^+, so that only bin-to-bin variations are apparent. Some of those for $B^\pm \to DK^\pm$ are significant, and exhibit a non-trivial distribution, which is driven by the variation in the strong-phase difference between D^0 and $\overline{D}^0$ decays. In the $B^\pm \to D\pi^\pm$ mode, there is a lower sensitivity to *CP* violation and therefore no such behaviour is seen. Under the hypothesis that the fit model is correct, p-values for Fig. 4a and Fig. 4b, based on statistical uncertainties only, are 0.95 and 0.05, respectively.

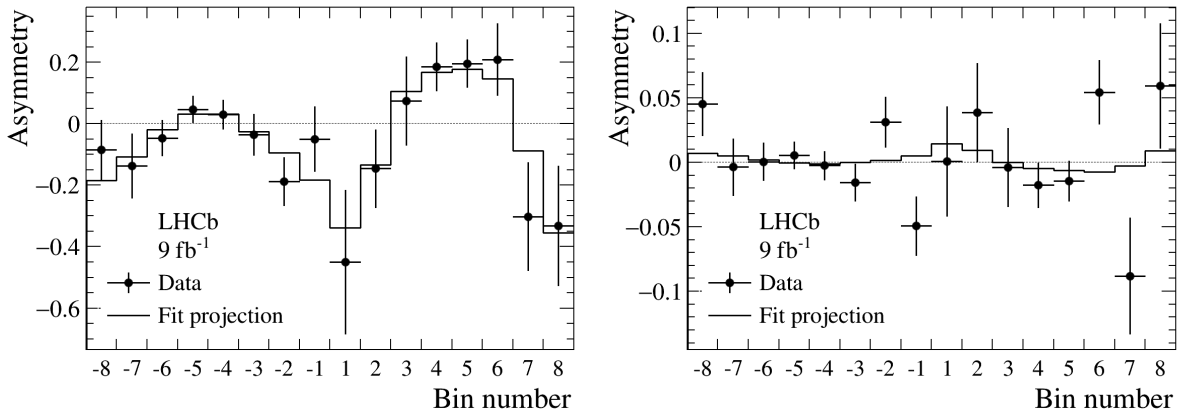

(a) $B^\pm \to DK^\pm$. (b) $B^\pm \to D\pi^\pm$.

Figure 4: The $B^\pm \to [K^+K^-\pi^+\pi^-]_D h^\pm$ fractional bin asymmetries in each phase-space bin. The solid black line is the prediction using the fitted *CP*-violating observables. The dotted line indicates the asymmetry prediction in the absence of *CP* violation.

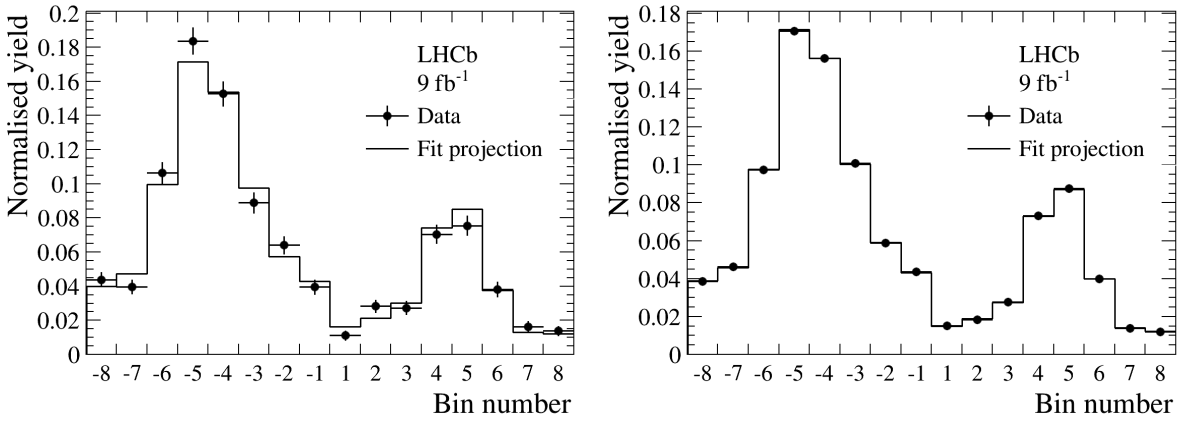

(a) $B^\pm \to DK^\pm$. (b) $B^\pm \to D\pi^\pm$.

Figure 5: The $B^\pm \to [K^+K^-\pi^+\pi^-]_D h^\pm$ total bin yields in each phase-space bin, and the predictions using the fitted *CP*-violating observables.

As a cross check, the total bin yields $N_i^- + N_{-i}^+$ are also shown in Fig. 5, where the sum over all bins is normalised to unity. The predictions from the fit results are also plotted, and reasonable agreement is found. Pseudoexperiments indicate that the p-values of Fig. 5a and 5b are highly correlated, and their combined p-value is 0.04, accounting for statistical uncertainties only.

To determine the phase-space integrated *CP*-violating observables, an analogous fit is performed without phase-space binning. The $B^\pm \to [K^+K^-\pi^+\pi^-]_D h^\pm$ and $B^\pm \to [\pi^+\pi^-\pi^+\pi^-]_D h^\pm$ modes are fitted simultaneously, and the yields, split by charge, are expressed in terms of the *CP*-violating observables. The shape parameters of the signal and background contributions are common fit parameters between the two D-decay channels. The fits to the invariant-mass distributions for the $B^\pm$ candidates are shown in Figs. 6 and 7, split by B decay, D decay and charge, and the resulting *CP*-violating observables

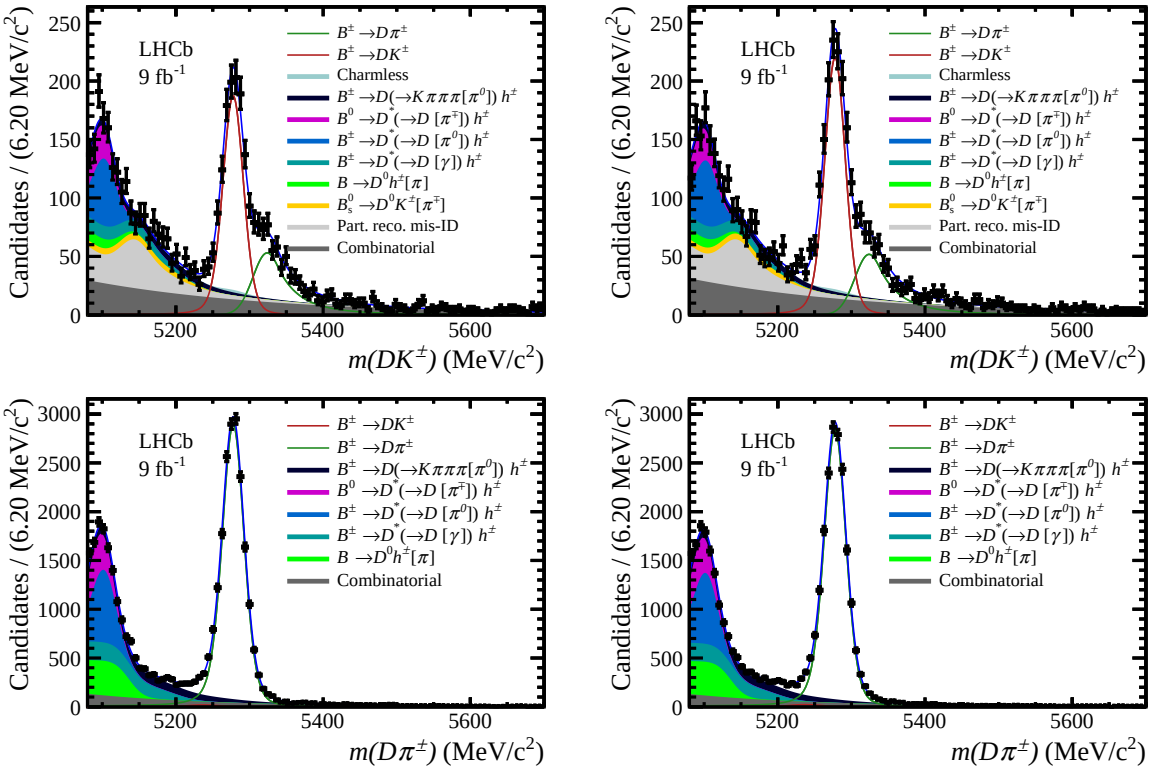

Figure 6: Invariant-mass distributions and fit projections of $B^{\pm} \to [K^+K^-\pi^+\pi^-]_D K^{\pm}$ (top) and $B^{\pm} \to [K^+K^-\pi^+\pi^-]_D \pi^{\pm}$ (bottom) candidates, divided between B^+ (left) and B^- (right).

Table 4: *CP*-violating observables of the phase-space integrated measurements. The first uncertainty is statistical, and the second systematic.

CP-violating observable	Value
$A_K^{KK\pi\pi}$	$0.093 \pm 0.023 \pm 0.002$
$A_\pi^{KK\pi\pi}$	$-0.009 \pm 0.006 \pm 0.001$
$A_K^{\pi\pi\pi\pi}$	$0.060 \pm 0.013 \pm 0.001$
$A_\pi^{\pi\pi\pi\pi}$	$-0.0082 \pm 0.0031 \pm 0.0007$
$R_{CP}^{KK\pi\pi}$	$0.974 \pm 0.024 \pm 0.015$
$R_{CP}^{\pi\pi\pi\pi}$	$0.978 \pm 0.014 \pm 0.010$

are listed in Table 4. These results are corrected for production asymmetries of the $B^{\pm}$ mesons and detection asymmetries of the companion hadron, using values reported in Ref. [7]. The measured values of the observables of the $B^{\pm} \to [\pi^+\pi^-\pi^+\pi^-]_D h^{\pm}$ mode are consistent with those reported in Ref. [4].

7 Systematic uncertainties

The systematic uncertainties in the binned measurement are summarised in Table 5. The uncertainties arise both from contributions that are internal to the analysis, and also from

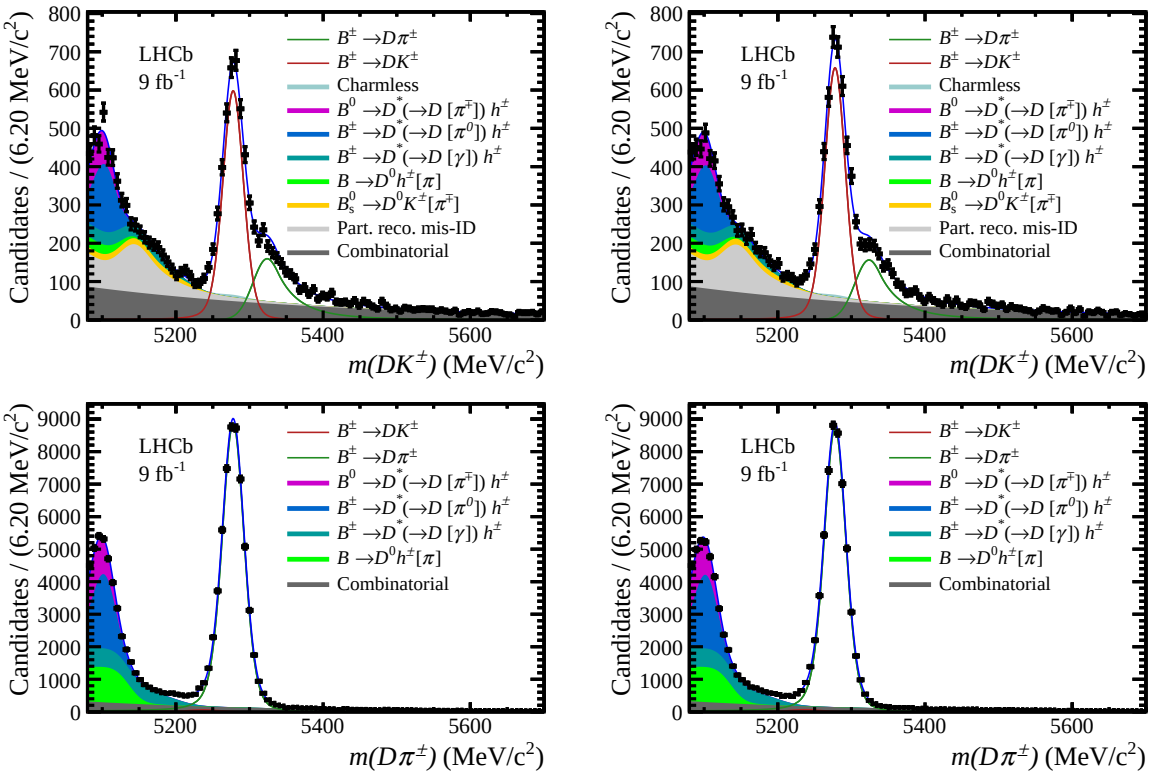

Figure 7: Invariant-mass distributions and fit projections of $B^{\pm} \to [\pi^+\pi^-\pi^+\pi^-]_D K^{\pm}$ (top) and $B^{\pm} \to [\pi^+\pi^-\pi^+\pi^-]_D \pi^{\pm}$ (bottom) candidates, divided between B^+ (left) and B^- (right).

knowledge of the c_i and s_i parameters, that come from an external source.

The uncertainties associated with the fixed invariant-mass shapes are propagated to the *CP*-violating observables by repeating the two-stage fit procedure many times, with different choices of shape. For each iteration, the shape parameters that are fixed in the global fit are changed to new values obtained with a resampling technique and the global fit rerun. The other shape parameters that are determined from this fit are then input to the binned fit, which is otherwise unchanged from the baseline configuration. The standard deviations of the resulting distributions of the *CP*-violating observables are assigned as the systematic uncertainties due to fixed mass shapes. Furthermore, to assess the impact of any bin-dependence of the mass shapes, the mass shapes are determined separately in each bin and pseudoexperiments are generated with individual mass shapes in each bin. The shifts in results are taken as the corresponding systematic uncertainties.

The uncertainties on the PID efficiencies are propagated to $x_{\pm}^{DK}$, $y_{\pm}^{DK}$, $x_{\xi}^{D\pi}$ and $y_{\xi}^{D\pi}$ by repeating the fit to the *CP*-violating observables, each time varying the parameters within their uncertainties. The same procedure is followed to assign the uncertainties associated with the relative contributions of the different components of the low-mass partially reconstructed background. Similarly, for the charmless background, the yields are varied within their uncertainties. The standard deviations of the fitted *CP*-violating observables are taken as the systematic uncertainties.

The partially reconstructed background at low mass is subject to *CP* violation that means the bin distribution of these events differs between the B^+ and B^- samples. To investigate this effect, pseudoexperiments are generated containing *CP* violation for these

decays, following the procedure described in Ref. [6], which are then fitted using the baseline model. The observed shifts in results are taken as the systematic uncertainties from this source.

There are several known sources of background lying in the signal region that are not accounted for in the invariant-mass fit. These are semi-leptonic b-hadron decays that survive the muon veto; $B^\pm \to Dh^\pm$ decays where the D meson decays semi-leptonically; $B^\pm \to Dh^\pm$, $D \to K^\mp\pi^\pm\pi^+\pi^-$ decays, where the kaon is misidentified as a pion, and two of the pions are misidentified as kaons; and $\Lambda_b^0 \to pD^0\pi^-$ (and charge conjugated case), where the p is misidentified as the companion hadron and the pion is not reconstructed. To evaluate the potential bias arising from these neglected contributions, pseudoexperiments are generated with each component included, which are then fitted with the baseline model. The shifts in the resulting *CP*-violating observables are taken as the systematic uncertainties.

The distribution of $D \to K^\mp\pi^\pm\pi^+\pi^-\pi^0$ background over phase space is not well known. The impact of this lack of knowledge is assessed by changing the distribution from that of the baseline model to one in which the population in each bin is proportional to the F_i parameters. The shifts in the *CP*-violating observables are assigned as the systematic uncertainties.

Finally, systematic uncertainties due to fit biases are included, which are set to be equal to the size of the bias for each *CP*-violating observable. Adding these in quadrature to the contributions discussed above gives a total LHCb systematic uncertainty for each observable that is an order of magnitude smaller than the corresponding statistical uncertainty.

In the current analysis the values of the c_i and s_i parameters are taken from the amplitude model constructed with LHCb data and described in Ref. [17]. An alternative model fitted to data from the CLEO experiment [41] is used to generate pseudoexperiments which are then fitted using the c_i and s_i parameters from the LHCb model. The observed shifts in the *CP*-violating observables are taken as the uncertainties arising from the choice of model used to calculate the c_i and s_i parameters. These uncertainties are in several cases significantly larger than the LHCb systematic uncertainties. In the future, the values of c_i and s_i will be taken from measurements performed at charm threshold, which will affect both the central values of the observables and allow the corresponding uncertainties to be assigned in a model-independent manner.

Cross checks are performed with simulation that validate certain assumptions in the analysis, and for which no systematic uncertainties are therefore applied. These studies assess the difference in acceptance over D-meson phase space for $B^\pm \to DK^\pm$ and $B^\pm \to D\pi^\pm$ decays, acceptance effects on the effective values of c_i and s_i, the effects of bin migration, and the neglect of D^0-$\overline{D}^0$ mixing in the fit. In all cases there are negligible biases on the measured parameters, within the current statistical precision.

It should be noted that the binned measurement is largely insensitive to D^0-$\overline{D}^0$ mixing and bin migration because F_i are free parameters in the fit. Since the mixing and bin-migration effects are very similar between the $B^\pm \to DK^\pm$ and $B^\pm \to D\pi^\pm$ modes, the $B^\pm \to D\pi^\pm$ mode provides a first order correction that is incorporated into the F_i parameters.

The systematic uncertainties on the phase-space integrated observables are shown in Table 6. They are evaluated using the same strategy as those in the binned analysis. In addition, there are systematic uncertainties due to the production and detection

Table 5: Summary of statistical and systematic uncertainties, multiplied by 10^2, on the *CP*-violating observables in the binned analysis.

Source	x_-^{DK}	y_-^{DK}	x_+^{DK}	y_+^{DK}	$x_\xi^{D\pi}$	$y_\xi^{D\pi}$
Mass shape	0.02	0.02	0.03	0.06	0.02	0.04
Bin-dependent mass shape	0.11	0.05	0.10	0.19	0.68	0.16
PID efficiency	0.02	0.02	0.03	0.06	0.02	0.04
Low-mass background model	0.02	0.02	0.03	0.04	0.02	0.02
Charmless background	0.14	0.15	0.12	0.14	0.01	0.02
CP violation in low-mass background	0.01	0.10	0.08	0.12	0.07	0.26
Semi-leptonic b-hadron decays	0.05	0.27	0.06	0.01	0.07	0.19
Semi-leptonic charm decays	0.02	0.07	0.03	0.15	0.06	0.24
$D \to K^\mp\pi^\pm\pi^+\pi^-$ background	0.11	0.05	0.07	0.04	0.09	0.05
$\Lambda_b^0 \to pD\pi^-$ background	0.01	0.25	0.14	0.04	0.06	0.34
$D \to K^\mp\pi^\pm\pi^+\pi^-\pi^0$ background	0.30	0.05	0.19	0.07	0.05	0.01
Fit bias	0.06	0.05	0.13	0.02	0.06	0.13
Total LHCb systematic	0.37	0.43	0.34	0.32	0.70	0.57
c_i, s_i	0.35	3.64	1.74	1.29	0.14	1.10
Total systematic	0.51	3.67	1.78	1.33	0.72	1.24
Statistical	2.87	3.40	2.51	3.05	4.24	5.17

Table 6: Summary of statistical and systematic uncertainties, multiplied by 10^3, on the *CP*-violating observables in the phase-space integrated analysis

Source	$A_K^{KK\pi\pi}$	$A_\pi^{KK\pi\pi}$	$A_K^{\pi\pi\pi\pi}$	$A_\pi^{\pi\pi\pi\pi}$	$R_{CP}^{KK\pi\pi}$	$R_{CP}^{\pi\pi\pi\pi}$
Charmless background	1.2	< 0.1	0.4	< 0.1	13.9	8.5
External parameters	1.0	0.7	1.0	0.7	4.0	4.0
Fixed yield fractions	0.1	< 0.1	0.1	< 0.1	1.3	1.4
Mass shape	0.3	< 0.1	0.2	< 0.1	3.1	3.1
PID efficiency	0.1	< 0.1	0.1	< 0.1	2.5	1.6
Total systematic	1.6	0.7	1.1	0.7	15.1	10.1
Statistical	23.5	5.5	13.3	3.1	24.2	14.3

asymmetries, which are estimated by repeating the fit many times, each time varying the parameters within their uncertainties [7], and taking the spreads of the resulting distributions as the assigned uncertainties. The total systematic uncertainties for the asymmetries are an order of magnitude smaller than the statistical uncertainties, and of a similar size for the ratio observables.

Correlation matrices for all the measured observables can be found in Appendix B.

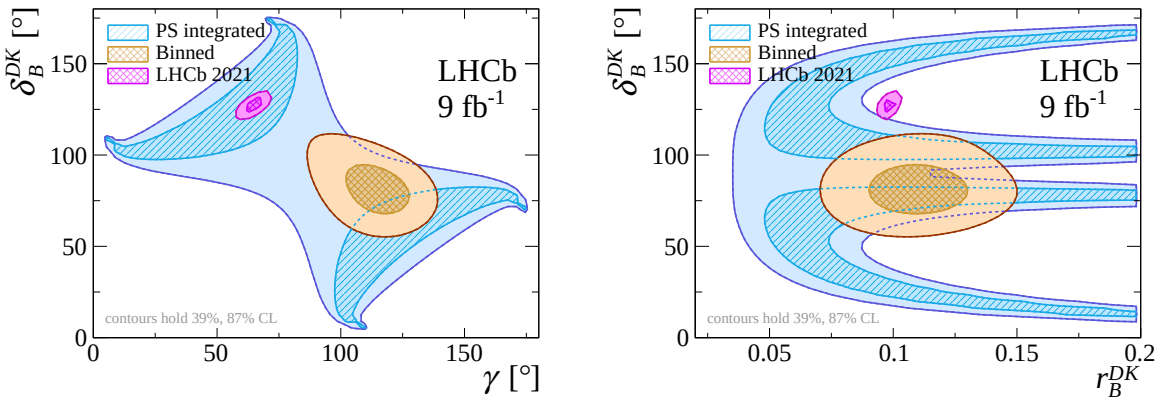

(a) γ vs δ_B^{DK}. (b) r_B^{DK} vs δ_B^{DK}.

Figure 8: Interpretation of the binned and phase-space ('PS') integrated measurements in terms to the underlying physics parameters, showing the 1 and 2σ contours. Also shown is the result from the analysis of other decay modes at LHCb ('LHCb 2021') [20].

8 Interpretation

The measured *CP*-violating observables in Table 3 are interpreted in terms of the underlying physics parameters γ, δ_B^{DK}, r_B^{DK}, $\delta_B^{D\pi}$ and $r_B^{D\pi}$ using a maximum likelihood fit, following the procedure described in Ref. [20].

The fit is first made to the results of the $B^\pm \to [K^+K^-\pi^+\pi^-]_D h^\pm$ binned analysis alone. The 1 and 2σ contours in the γ vs. δ_B^{DK} and the r_B^{DK} vs. δ_B^{DK} planes are shown in Fig. 8. The numerical results are

$$\begin{aligned}
\gamma &= (116^{+12}_{-14})^\circ, \\
\delta_B^{DK} &= (81^{+14}_{-13})^\circ, \\
r_B^{DK} &= 0.110^{+0.020}_{-0.020}, \\
\delta_B^{D\pi} &= (298^{+62}_{-118})^\circ, \\
r_B^{D\pi} &= 0.0041^{+0.0054}_{-0.0041},
\end{aligned}$$

where the uncertainties are the combined statistical and systematic uncertainties. These results may be compared to those from a recent measurement of γ and associated parameter derived from an ensemble of beauty and charm-meson decay studies performed by LHCb [20]. The 3σ contours of the results for γ and δ_B^{DK} from the $B^\pm \to [K^+K^-\pi^+\pi^-]_D h^\pm$ analysis encompass the central values coming from the other decay modes. There is good agreement between the two measurements for the r_B^{DK}, $\delta_B^{D\pi}$ and $r_B^{D\pi}$ parameters.

The fit is then made to the phase-space inclusive *CP*-violating observables. Here it is necessary to know the *CP*-even fractions F_+ for each decay. In the case of $D \to K^+K^-\pi^+\pi^-$ this is taken as 0.736, as calculated from the LHCb amplitude model [17]. For $D \to \pi^+\pi^-\pi^+\pi^-$ the value of 0.735 ± 0.016 is used, as measured by the BESIII collaboration [42]. Due to the trigonometric dependence, multiple solutions are obtained. The likelihood contours are shown in Fig. 8. It can be seen that these have regions that are compatible with the result coming from the other decay channels.

9 Summary and conclusions

The first measurement of *CP*-violating observables for the decay $B^\pm \to [K^+K^-\pi^+\pi^-]_D h^\pm$ has been presented. The analysis is performed in bins of phase space of the D-meson decay, which are chosen to optimise sensitivity to the angle γ of the CKM Unitary Triangle. The local asymmetries confirm the presence of *CP* violation effects that have also been observed in other $B^\pm \to DK^\pm$ decay modes. In addition, measurements of *CP*-violating observables integrated over phase space are performed for the decays $B^\pm \to [K^+K^-\pi^+\pi^-]_D h^\pm$ and $B^\pm \to [\pi^+\pi^-\pi^+\pi^-]_D h^\pm$. All studies make use of the full data set collected by LHCb in Run 1 and 2. The measurement of the inclusive observables in $B^\pm \to [\pi^+\pi^-\pi^+\pi^-]_D h^\pm$ supersede those reported in Ref. [7].

The measurements of the *CP*-violating observables in the binned analysis require knowledge of the D-meson strong-phase parameters c_i and s_i. The values of these parameters are currently taken from an amplitude model [17]. In the future, direct measurements of these parameters at charm threshold [21] in combination with the measured yields in each bin, which are reported in Appendix A, will allow the *CP*-violating observables to be re-determined in a model-independent fashion.

The current measurements, together with those of the inclusive charge asymmetries, may be interpreted in terms of γ and the other underlying physics parameters. When this is done for the results of the binned $B^\pm \to [K^+K^-\pi^+\pi^-]_D h^\pm$ analysis, a value of $\gamma = (116^{+12}_{-14})^\circ$ is obtained. This result will evolve when the observables are re-evaluated using model-independent inputs. A model-independent determination of γ making use of both the binned and unbinned analysis of these four-body D-meson decay modes will be a valuable addition to the set of measurements of this important parameter already performed at LHCb. The precision of the four-body D-decay studies is limited by the sample size and is expected to improve significantly with future data from LHCb.

Acknowledgements

We express our gratitude to our colleagues in the CERN accelerator departments for the excellent performance of the LHC. We thank the technical and administrative staff at the LHCb institutes. We acknowledge support from CERN and from the national agencies: CAPES, CNPq, FAPERJ and FINEP (Brazil); MOST and NSFC (China); CNRS/IN2P3 (France); BMBF, DFG and MPG (Germany); INFN (Italy); NWO (Netherlands); MNiSW and NCN (Poland); MEN/IFA (Romania); MSHE (Russia); MICINN (Spain); SNSF and SER (Switzerland); NASU (Ukraine); STFC (United Kingdom); DOE NP and NSF (USA). We acknowledge the computing resources that are provided by CERN, IN2P3 (France), KIT and DESY (Germany), INFN (Italy), SURF (Netherlands), PIC (Spain), GridPP (United Kingdom), RRCKI and Yandex LLC (Russia), CSCS (Switzerland), IFIN-HH (Romania), CBPF (Brazil), PL-GRID (Poland) and NERSC (USA). We are indebted to the communities behind the multiple open-source software packages on which we depend. Individual groups or members have received support from ARC and ARDC (Australia); Minciencias (Colombia); AvH Foundation (Germany); EPLANET, Marie Skłodowska-Curie Actions and ERC (European Union); A*MIDEX, ANR, IPhU and Labex P2IO, and Région Auvergne-Rhône-Alpes (France); Key Research Program of Frontier Sciences of CAS, CAS PIFI, CAS CCEPP, Fundamental Research Funds for the

Central Universities, and Sci. & Tech. Program of Guangzhou (China); RFBR, RSF and Yandex LLC (Russia); GVA, XuntaGal and GENCAT (Spain); SRC (Sweden); the Leverhulme Trust, the Royal Society and UKRI (United Kingdom).

Appendices

A Alternative binning scheme and yields in bins of phase space

The fitted parameters $x_{\pm}^{DK}$, $y_{\pm}^{DK}$, $x_{\xi}^{D\pi}$ and $y_{\xi}^{D\pi}$ are determined using values of c_i and s_i calculated from an amplitude model. When direct measurements of c_i and s_i are available from studies at charm threshold it will be desirable to update the $B^{\pm} \to [K^+K^-\pi^+\pi^-]_D h^{\pm}$ binned analysis with this information as input. In order to enable this re-analysis an alternative fit is carried where the yields in each bin are fitted, instead of the *CP*-violating observables.

The bin yields for the 2×8 scheme is presented in Sec. A.1. Furthermore, it is possible that the sample sizes at charm threshold may be smaller than foreseen. In that case a 2×4 binning scheme might be more suited to the analysis. Therefore, in this Appendix a 2×4 binning scheme is presented in Sec. A.2 together with the bin yields and essential information for this scheme. The corresponding correlation matrices are available in Ref. [43].

A.1 2×8 bins

Table 7 lists the bin yields for the 2×8 binning scheme.

When the *CP* observables are determined from the bin yields, rather than as an output of the fit to the invariant-mass spectrum, the fit biases change. The biases with this new configuration, which should be used to correct the observables and replace the corresponding systematic uncertainty in Table 5, are presented in Table 8. The new correlation matrix for systematic uncertainties is presented in Table 9, which only contains contributions from internal systematic uncertainties.

A.2 2×4 bins

The 2×4 binning scheme is presented in Fig. 9, and the corresponding c_i, s_i and F_i parameters, and the normalised bin volumes V_i calculated from the model, are listed in Table 10. The optimised Q-value is $Q = 0.85$. The code provided in Ref. [26] can be used to assign bin numbers to D decays with this binning scheme as well.

Table 11 lists the bin yields for the 2×4 binning scheme. Additionally, the internal systematic uncertainties, evaluated for a 2×4 binning scheme, are also provided in Table 12, which are evaluated in an identical manner to those found in Table 5. The correlation matrix of the systematic uncertainties is given in Table 13.

Table 7: The bin yields with the 2×8 binning scheme.

Bin	$B^- \to DK^-$	$B^+ \to DK^+$	$B^- \to D\pi^-$	$B^+ \to D\pi^+$
8	17 ± 6	74 ± 10	312 ± 21	920 ± 34
7	21 ± 7	71 ± 10	309 ± 21	1160 ± 37
6	81 ± 12	173 ± 15	1025 ± 36	2422 ± 53
5	157 ± 15	271 ± 19	2103 ± 50	4226 ± 68
4	146 ± 15	230 ± 17	1750 ± 46	3899 ± 66
3	52 ± 9	143 ± 14	671 ± 30	2554 ± 54
2	43 ± 9	120 ± 13	468 ± 25	1417 ± 41
1	11 ± 6	65 ± 10	369 ± 22	1137 ± 37
-1	66 ± 10	26 ± 7	1009 ± 35	376 ± 23
-2	93 ± 12	51 ± 9	1477 ± 41	442 ± 25
-3	152 ± 15	39 ± 9	2424 ± 53	690 ± 30
-4	277 ± 19	88 ± 12	3800 ± 65	1851 ± 47
-5	339 ± 21	93 ± 13	4185 ± 68	2210 ± 50
-6	180 ± 15	46 ± 9	2375 ± 52	939 ± 34
-7	61 ± 10	34 ± 8	1127 ± 36	376 ± 23
-8	71 ± 10	29 ± 7	987 ± 34	283 ± 20

Table 8: Fit bias when using the bin yields, multiplied by 10^2, for a 2×8 binning scheme.

x_-^{DK}	y_-^{DK}	x_+^{DK}	y_+^{DK}	$x_\xi^{D\pi}$	$y_\xi^{D\pi}$
0.26	0.11	0.12	0.04	0.21	0.10

B Correlation matrices for *CP*-violating observables

The statistical and systematic correlation matrices of the *CP*-violating observables from the binned and phase-space integrated measurements are shown in Tables 14-17. Tables 14 and 15 include contributions from c_i and s_i, which are currently model dependent.

Table 9: Systematic correlation matrix of *CP*-violating observables for the binned measurement, with a 2×8 binning scheme. The contribution from c_i and s_i has been excluded.

x_-^{DK}	y_-^{DK}	x_+^{DK}	y_+^{DK}	$x_\xi^{D\pi}$	$y_\xi^{D\pi}$
1.000	0.010	0.572	0.411	-0.258	-0.127
0.010	1.000	0.099	0.083	-0.010	0.282
0.572	0.099	1.000	0.397	-0.158	0.119
0.411	0.083	0.397	1.000	-0.541	-0.461
-0.258	-0.010	-0.158	-0.541	1.000	0.269
-0.127	0.282	0.119	-0.461	0.269	1.000

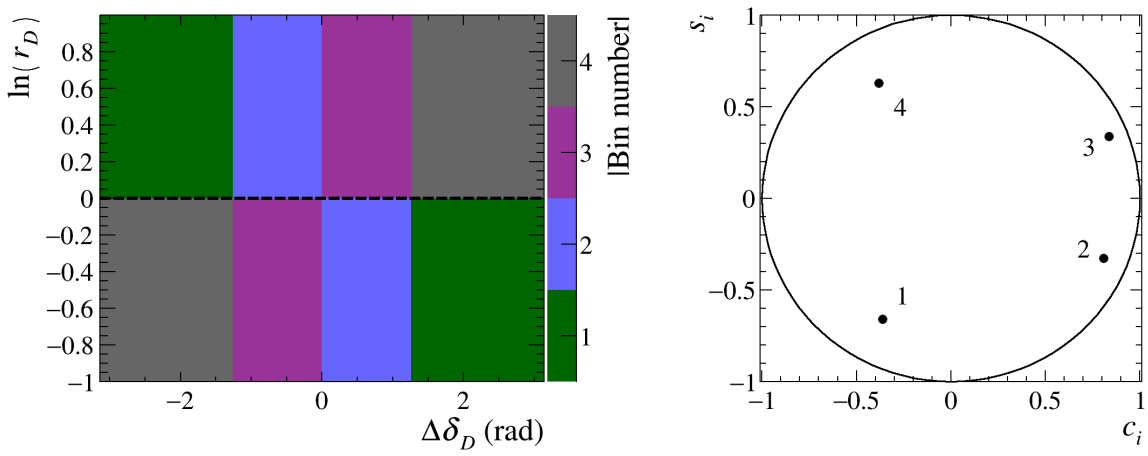

(a) 2×4 binning scheme.

(b) c_i and s_i

Figure 9: The optimised 2×4 binning scheme in $\Delta\delta_D$-ln(r_D) space and the associated c_i and s_i parameters calculated using the amplitude model.

Table 10: c_i, s_i, F_i and V_i for the optimised 2×4 binning scheme, as calculated from the amplitude model.

Bin number	c_i	s_i	F_i	F_{-i}	V_i	V_{-i}
1	−0.3623	−0.6585	0.0327	0.1085	0.1152	0.1153
2	0.8038	−0.3325	0.0997	0.2544	0.1455	0.1455
3	0.8341	0.3387	0.1225	0.2656	0.1442	0.1442
4	−0.3862	0.6269	0.0263	0.0902	0.0950	0.0950

Table 11: The bin yields with the 2×4 binning scheme.

Bin	$B^- \to DK^-$	$B^+ \to DK^+$	$B^- \to D\pi^-$	$B^+ \to D\pi^+$
4	36 ± 9	140 ± 14	600 ± 29	1969 ± 49
3	240 ± 19	448 ± 25	3140 ± 62	6753 ± 87
2	197 ± 18	374 ± 23	2452 ± 55	6561 ± 86
1	50 ± 10	181 ± 16	799 ± 33	2436 ± 54
−1	153 ± 15	76 ± 12	2376 ± 53	792 ± 33
−2	436 ± 25	130 ± 15	6332 ± 85	2559 ± 56
−3	528 ± 26	142 ± 16	6649 ± 87	3177 ± 62
−4	122 ± 14	60 ± 10	2022 ± 49	626 ± 30

Table 12: Summary of all systematic uncertainties of *CP*-violating observables for the binned measurement, multiplied by 10^2, with a 2×4 binning scheme.

Source	x_-^{DK}	y_-^{DK}	x_+^{DK}	y_+^{DK}	$x_\xi^{D\pi}$	$y_\xi^{D\pi}$
Mass shape	0.01	0.01	0.02	0.04	0.02	0.03
Bin-dependent mass shape	0.31	0.43	0.36	0.10	0.40	0.01
PID efficiency	0.01	0.01	0.02	0.04	0.02	0.03
Low-mass background model	0.01	0.01	0.01	0.01	0.03	0.01
Charmless background	0.11	0.17	0.09	0.14	0.01	0.01
CP violation in low-mass background	0.05	0.22	0.07	0.14	0.15	0.13
Semi-leptonic b-hadron decays	0.07	0.08	0.03	0.07	0.17	0.56
Semi-leptonic charm decays	0.02	0.01	0.04	0.02	0.15	0.29
$D \to K^\mp\pi^\pm\pi^+\pi^-$ background	0.02	0.09	0.01	0.06	0.25	0.61
$\Lambda_b^0 \to pD\pi^-$ background	0.16	0.04	0.13	0.04	0.01	0.12
$D \to K^\mp\pi^\pm\pi^+\pi^-\pi^0$ background	0.09	0.11	0.44	0.08	0.12	0.46
Fit bias	0.19	0.27	0.07	0.19	0.51	0.21
Total LHCb systematic	0.43	0.60	0.61	0.32	0.76	1.03

Table 13: Systematic correlation matrix of *CP*-violating observables for the binned mesaurement, with a 2×4 binning scheme. The contribution from c_i and s_i has been excluded.

x_-^{DK}	y_-^{DK}	x_+^{DK}	y_+^{DK}	$x_\xi^{D\pi}$	$y_\xi^{D\pi}$
1.000	−0.591	0.742	−0.329	−0.504	0.290
−0.591	1.000	−0.388	0.622	0.388	0.036
0.742	−0.388	1.000	−0.586	−0.250	0.355
−0.329	0.622	−0.586	1.000	0.067	−0.000
−0.504	0.388	−0.250	0.067	1.000	−0.043
0.290	0.036	0.355	−0.000	−0.043	1.000

Table 14: Statistical correlation matrix of *CP*-violating observables for the binned measurement.

x_-^{DK}	y_-^{DK}	x_+^{DK}	y_+^{DK}	$x_\xi^{D\pi}$	$y_\xi^{D\pi}$
1.000	0.032	0.008	−0.010	0.034	0.102
0.032	1.000	0.017	−0.000	−0.091	0.080
0.008	0.017	1.000	0.007	−0.100	0.051
−0.010	−0.000	0.007	1.000	0.012	−0.097
0.034	−0.091	−0.100	0.012	1.000	0.014
0.102	0.080	0.051	−0.097	0.014	1.000

Table 15: Systematic correlation matrix of *CP*-violating observables for the binned measurement.

x_-^{DK}	y_-^{DK}	x_+^{DK}	y_+^{DK}	$x_\xi^{D\pi}$	$y_\xi^{D\pi}$
1.000	−0.678	0.751	0.736	−0.048	−0.650
−0.678	1.000	−0.973	−0.961	−0.200	0.898
0.751	−0.973	1.000	0.971	0.166	−0.862
0.736	−0.961	0.971	1.000	0.065	−0.913
−0.048	−0.200	0.166	0.065	1.000	−0.057
−0.650	0.898	−0.862	−0.913	−0.057	1.000

Table 16: Statistical correlation matrix of *CP*-violating observables for the phase-space integrated measurement.

$A_K^{KK\pi\pi}$	$A_\pi^{KK\pi\pi}$	$A_K^{\pi\pi\pi\pi}$	$A_\pi^{\pi\pi\pi\pi}$	$R_{\rm CP}^{KK\pi\pi}$	$R_{\rm CP}^{\pi\pi\pi\pi}$
1.000	−0.025	0.000	−0.000	0.015	0.000
−0.025	1.000	0.000	−0.000	0.002	0.000
0.000	0.000	1.000	−0.028	0.002	0.016
−0.000	−0.000	−0.028	1.000	0.000	0.002
0.015	0.002	0.002	0.000	1.000	0.068
0.000	0.000	0.016	0.002	0.068	1.000

Table 17: Systematic correlation matrix of *CP*-violating observables for the phase space inclusive measurement.

$A_K^{KK\pi\pi}$	$A_\pi^{KK\pi\pi}$	$A_K^{\pi\pi\pi\pi}$	$A_\pi^{\pi\pi\pi\pi}$	$R_{CP}^{KK\pi\pi}$	$R_{CP}^{\pi\pi\pi\pi}$
1.000	0.442	0.594	0.441	−0.723	−0.060
0.442	1.000	0.646	0.999	0.002	0.008
0.594	0.646	1.000	0.643	−0.042	−0.348
0.441	0.999	0.643	1.000	0.009	0.013
−0.723	0.002	−0.042	0.009	1.000	0.236
−0.060	0.008	−0.348	0.013	0.236	1.000

References

[1] N. Cabibbo, *Unitary symmetry and leptonic decays*, Phys. Rev. Lett. **10** (1963) 531.

[2] M. Kobayashi and T. Maskawa, *CP-violation in the renormalizable theory of weak interaction*, Prog. Theor. Phys. **49** (1973) 652.

[3] J. Brod and J. Zupan, *The ultimate theoretical error on γ from $B \to DK$ decays*, JHEP **01** (2014) 051, arXiv:1308.5663.

[4] LHCb collaboration, R. Aaij *et al.*, *Measurement of CP observables in $B^\pm \to DK^\pm$ and $B^\pm \to D\pi^\pm$ with two- and four-body D decays*, Phys. Lett. **B760** (2016) 117, arXiv:1603.08993.

[5] LHCb collaboration, R. Aaij *et al.*, *Measurement of CP observables in $B^\pm \to DK^\pm$ and $B^\pm \to D\pi^\pm$ with $D \to K^0_S K^\pm \pi^\mp$ decays*, JHEP **06** (2020) 58, arXiv:2002.08858.

[6] LHCb collaboration, R. Aaij *et al.*, *Measurement of the CKM angle γ in $B^\pm \to DK^\pm$ and $B^\pm \to D\pi^\pm$ decays with $D \to K^0_S h^+ h^-$*, JHEP **02** (2021) 0169, arXiv:2010.08483.

[7] LHCb collaboration, R. Aaij *et al.*, *Measurement of CP observables in $B^\pm \to D^{(*)}K^\pm$ and $B^\pm \to D^{(*)}\pi^\pm$ decays using two-body D final states*, JHEP **04** (2021) 081, arXiv:2012.09903.

[8] LHCb collaboration, R. Aaij *et al.*, *Constraints on the CKM angle γ from $B^\pm \to Dh^\pm$ decays using $D \to h^\pm h'^\mp \pi^0$ final states*, JHEP **07** (2022) 099, arXiv:2112.10617.

[9] BaBar collaboration, P. del Amo Sanchez *et al.*, *Evidence for direct CP violation in the measurement of the Cabibbo-Kobayashi-Maskawa angle γ with $B^\mp \to D^{(*)}K^{(*)\mp}$ decays*, Phys. Rev. Lett. **105** (2010) 121801, arXiv:1005.1096.

[10] Belle collaboration, P. K. Resmi *et al.*, *First measurement of the CKM angle ϕ_3 with $B^\pm \to D(K^0_S\pi^+\pi^-\pi^0)K^\pm$ decays*, JHEP **10** (2019) 178, arXiv:1908.09499.

[11] Belle and Belle II collaborations, F. Abudinén *et al.*, *Combined analysis of Belle and Belle II data to determine the CKM angle ϕ_3 using $B^+ \to D(K^0_S h^- h^+)h^+$ decays*, JHEP **02** (2022) 063, arXiv:2110.12125.

[12] A. Bondar, *Proceedings of BINP special analysis meeting on Dalitz analysis, 24-26 Sep. 2002*, unpublished (2002).

[13] A. Bondar and A. Poluektov, *Feasibility study of model-independent approach to ϕ_3 measurement using Dalitz plot analysis*, Eur. Phys. J. **C47** (2006) 347, arXiv:hep-ph/0510246.

[14] A. Bondar and A. Poluektov, *The use of quantum-correlated D^0 decays for ϕ_3 measurement*, Eur. Phys. J. **C55** (2008) 51, arXiv:0801.0840.

[15] A. Giri, Y. Grossman, A. Soffer, and J. Zupan, *Determining γ using $B^\pm \to DK^\pm$ with multibody D decays*, Phys. Rev. **D68** (2003) 054018, arXiv:hep-ph/0303187.

[16] J. Rademacker and G. Wilkinson, *Determining the unitarity triangle angle γ with a four-body amplitude analysis of $B^\pm \to (K^+K^-\pi^+\pi^-)_D K^\pm$ decays*, Phys. Lett. **B647** (2007) 400, arXiv:hep-ph/0611272.

[17] LHCb collaboration, R. Aaij *et al.*, *Search for CP violation through an amplitude analysis of $D^0 \to K^+K^-\pi^+\pi^-$ decays*, JHEP **02** (2019) 126, arXiv:1811.08304.

[18] LHCb collaboration, R. Aaij *et al.*, *Measurement of the CKM angle γ with $B^\mp \to D[K^\pm\pi^\mp\pi^\mp\pi^\pm]h^\mp$ decays using a binned phase-space approach*, arXiv:2209.03692, submitted to JHEP.

[19] Heavy Flavor Averaging Group, Y. Amhis *et al.*, *Averages of b-hadron, c-hadron, and τ-lepton properties as of 2018*, Eur. Phys. J. **C81** (2021) 226, arXiv:1909.12524, updated results and plots available at https://hflav.web.cern.ch.

[20] LHCb collaboration, R. Aaij *et al.*, *Simultaneous determination of CKM angle γ and charm mixing parameters*, JHEP **12** (2021) 141, arXiv:2110.02350.

[21] BESIII collaboration, M. Ablikim *et al.*, *Future physics programme of BESIII*, Chin. Phys. C **44** (2020) 040001, arXiv:1912.05983.

[22] M. Nayak *et al.*, *First determination of the CP content of $D \to \pi^+\pi^-\pi^0$ and $D \to K^+K^-\pi^0$*, Phys. Lett. **B740** (2015) 1, arXiv:1410.3964.

[23] S. Malde *et al.*, *First determination of the CP content of $D \to \pi^+\pi^-\pi^+\pi^-$ and updated determination of the CP contents of $D \to \pi^+\pi^-\pi^0$ and $D \to K^+K^-\pi^0$*, Phys. Lett. **B747** (2015) 9, arXiv:1504.05878.

[24] M. Rama, *Effect of $D - \bar{D}$ mixing in the extraction of γ with $B^- \to D^0K^-$ and $B^- \to D^0\pi^-$ decays*, Phys. Rev. D **89** (2014) 014021, arXiv:1307.4384.

[25] S. Harnew *et al.*, *Model-independent determination of the strong phase difference between D^0 and $\overline{D}^0 \to \pi^+\pi^-\pi^+\pi^-$ amplitudes*, JHEP **01** (2018) 144, arXiv:1709.03467.

[26] M. Tat, *D0->KKpipi binning scheme*, 2022. doi: 10.5281/zenodo.6940031.

[27] LHCb collaboration, A. A. Alves Jr. *et al.*, *The LHCb detector at the LHC*, JINST **3** (2008) S08005.

[28] LHCb collaboration, R. Aaij *et al.*, *LHCb detector performance*, Int. J. Mod. Phys. **A30** (2015) 1530022, arXiv:1412.6352.

[29] T. Sjöstrand, S. Mrenna, and P. Skands, *A brief introduction to PYTHIA 8.1*, Comput. Phys. Commun. **178** (2008) 852, arXiv:0710.3820; T. Sjöstrand, S. Mrenna, and P. Skands, *PYTHIA 6.4 physics and manual*, JHEP **05** (2006) 026, arXiv:hep-ph/0603175.

[30] I. Belyaev *et al.*, *Handling of the generation of primary events in Gauss, the LHCb simulation framework*, J. Phys. Conf. Ser. **331** (2011) 032047.

[31] D. J. Lange, *The EvtGen particle decay simulation package*, Nucl. Instrum. Meth. **A462** (2001) 152.

[32] N. Davidson, T. Przedzinski, and Z. Was, *PHOTOS interface in C++: Technical and physics documentation*, Comp. Phys. Comm. **199** (2016) 86, arXiv:1011.0937.

[33] Geant4 collaboration, J. Allison *et al.*, *Geant4 developments and applications*, IEEE Trans. Nucl. Sci. **53** (2006) 270; Geant4 collaboration, S. Agostinelli *et al.*, *Geant4: A simulation toolkit*, Nucl. Instrum. Meth. **A506** (2003) 250.

[34] M. Clemencic *et al.*, *The LHCb simulation application, Gauss: Design, evolution and experience*, J. Phys. Conf. Ser. **331** (2011) 032023.

[35] D. Müller, M. Clemencic, G. Corti, and M. Gersabeck, *ReDecay: A novel approach to speed up the simulation at LHCb*, Eur. Phys. J. **C78** (2018) 1009, arXiv:1810.10362.

[36] L. Breiman, J. H. Friedman, R. A. Olshen, and C. J. Stone, *Classification and regression trees*, Wadsworth international group, Belmont, California, USA, 1984.

[37] Y. Freund and R. E. Schapire, *A decision-theoretic generalization of on-line learning and an application to boosting*, J. Comput. Syst. Sci. **55** (1997) 119.

[38] H. Voss, A. Hoecker, J. Stelzer, and F. Tegenfeldt, *TMVA - Toolkit for Multivariate Data Analysis with ROOT*, PoS **ACAT** (2007) 040; A. Hoecker *et al.*, *TMVA 4 — Toolkit for Multivariate Data Analysis with ROOT. Users Guide.*, arXiv:physics/0703039.

[39] LHCb collaboration, R. Aaij *et al.*, *Measurement of the CKM angle γ using $B^\pm \to DK^\pm$ with $D \to K^0_S\pi^+\pi^-$, $K^0_S K^+K^-$ decays*, JHEP **08** (2018) 176, Erratum ibid. **10** (2018) 107, arXiv:1806.01202.

[40] Particle Data Group, R. L. Workman *et al.*, *Review of particle physics*, Prog. Theor. Exp. Phys. **2022** (2022) 083C01.

[41] P. d'Argent *et al.*, *Amplitude analyses of $D^0 \to \pi^+\pi^-\pi^+\pi^-$ and $D^0 \to K^+K^-\pi^+\pi^-$ decays*, JHEP **05** (2017) 143, arXiv:1703.08505.

[42] BESIII collaboration, M. Ablikim *et al.*, *Measurement of the CP-even fraction of $D^0 \to \pi^+\pi^-\pi^+\pi^-$*, arXiv:2208.10098.

[43] LHCb collaboration, *$B^\pm \to Dh^\pm$, $D \to K^+K^-\pi^+\pi^-$ LHCb Run 1 and 2 bin yields*, 2022. doi: 10.5281/zenodo.xxx.

LHCb collaboration

R. Aaij[32], A.S.W. Abdelmotteleb[56], C. Abellán Beteta[50], F. Abudinén[56], T. Ackernley[60], B. Adeva[46], M. Adinolfi[54], P. Adlarson[87], H. Afsharnia[9], C. Agapopoulou[13], C.A. Aidala[88], Z. Ajaltouni[9], S. Akar[65], P. Albicocco[23], J. Albrecht[15], F. Alessio[48], M. Alexander[59], A. Alfonso Albero[45], Z. Aliouche[62], G. Alkhazov[38], P. Alvarez Cartelle[55], R. Amalric[13], S. Amato[2], J.L. Amey[54], Y. Amhis[11,48], L. An[48], L. Anderlini[22], M. Andersson[50], A. Andreianov[38], M. Andreotti[21], D. Andreou[68], D. Ao[6], F. Archilli[31], A. Artamonov[44], M. Artuso[68], E. Aslanides[10], M. Atzeni[50], B. Audurier[12], I.B Bachiller Perea[8], S. Bachmann[17], M. Bachmayer[49], J.J. Back[56], A. Bailly-reyre[13], P. Baladron Rodriguez[46], V. Balagura[12], W. Baldini[21,48], J. Baptista de Souza Leite[1], M. Barbetti[22,i], R.J. Barlow[62], S. Barsuk[11], W. Barter[58], M. Bartolini[55], F. Baryshnikov[84], J.M. Basels[14], G. Bassi[29,o], V. Batozskaya[36], B. Batsukh[4], A. Battig[15], A. Bay[49], A. Beck[56], M. Becker[15], F. Bedeschi[29,p], I. Bediaga[1], A. Beiter[68], S. Belin[46], V. Bellee[50], K. Belous[44], I. Belov[40], I. Belyaev[41], G. Benane[10], G. Bencivenni[23], E. Ben-Haim[13], A. Berezhnoy[40], R. Bernet[50], S. Bernet Andres[86], D. Berninghoff[17], H.C. Bernstein[68], C. Bertella[62], A. Bertolin[28], C. Betancourt[50], F. Betti[48], Ia. Bezshyiko[50], S. Bhasin[54], J. Bhom[35], L. Bian[74], M.S. Bieker[15], N.V. Biesuz[21], P. Billoir[13], A. Biolchini[32], M. Birch[61], F.C.R. Bishop[55], A. Bitadze[62], A. Bizzeti[22,m], M.P. Blago[55], T. Blake[56], F. Blanc[49], J.E. Blank[15], S. Blusk[68], D. Bobulska[59], V. Bocci[30], J.A. Boelhauve[15], O. Boente Garcia[12], T. Boettcher[65], A. Boldyrev[83], C.S. Bolognani[80], R. Bolzonella[21,h], A. Bondar[43], N. Bondar[38,48], F. Borgato[28], S. Borghi[62], M. Borsato[17], J.T. Borsuk[35], S.A. Bouchiba[49], T.J.V. Bowcock[60], A. Boyer[48], C. Bozzi[21], M.J. Bradley[61], S. Braun[66], A. Brea Rodriguez[46], J. Brodzicka[35], A. Brossa Gonzalo[46], J. Brown[60], D. Brundu[27], A. Buonaura[50], L. Buonincontri[28], A.T. Burke[62], C. Burr[48], A. Bursche[72], A. Butkevich[39], J.S. Butter[32], J. Buytaert[48], W. Byczynski[48], S. Cadeddu[27], H. Cai[74], R. Calabrese[21,h], L. Calefice[15], S. Cali[23], M. Calvi[26,l], M. Calvo Gomez[86], P. Campana[23], D.H. Campora Perez[80], A.F. Campoverde Quezada[6], S. Capelli[26,l], L. Capriotti[20], A. Carbone[20,f], R. Cardinale[24,j], A. Cardini[27], P. Carniti[26,l], L. Carus[14], K. Carvalho Akiba[32], A. Casais Vidal[46], R. Caspary[17], G. Casse[60], M. Cattaneo[48], G. Cavallero[61,48], V. Cavallini[21], S. Celani[49], J. Cerasoli[10], D. Cervenkov[63], A.J. Chadwick[60], I.C Chahrour[88], M.G. Chapman[54], M. Charles[13], Ph. Charpentier[48], C.A. Chavez Barajas[60], M. Chefdeville[8], C. Chen[10], S. Chen[4], A. Chernov[35], S. Chernyshenko[52], V. Chobanova[46], S. Cholak[49], M. Chrzaszcz[35], A. Chubykin[38], V. Chulikov[38], P. Ciambrone[23], M.F. Cicala[56], X. Cid Vidal[46], G. Ciezarek[48], P. Cifra[48], P.E.L. Clarke[58], M. Clemencic[48], H.V. Cliff[55], J. Closier[48], J.L. Cobbledick[62], V. Coco[48], J.A.B. Coelho[11], J. Cogan[10], E. Cogneras[9], L. Cojocariu[37], P. Collins[48], T. Colombo[48], L. Congedo[19], A. Contu[27], N. Cooke[53], I. Corredoira [46], G. Corti[48], B. Couturier[48], D.C. Craik[50], M. Cruz Torres[1,d], R. Currie[58], C.L. Da Silva[67], S. Dadabaev[84], L. Dai[71], X. Dai[5], E. Dall'Occo[15], J. Dalseno[46], C. D'Ambrosio[48], J. Daniel[9], A. Danilina[41], P. d'Argent[19], J.E. Davies[62], A. Davis[62], O. De Aguiar Francisco[62], J. De Boer[48], K. De Bruyn[79], S. De Capua[62], M. De Cian[49], U. De Freitas Carneiro Da Graca[1], E. De Lucia[23], J.M. De Miranda[1], L. De Paula[2], M. De Serio[19,e], D. De Simone[50], P. De Simone[23], F. De Vellis[15], J.A. de Vries[80], C.T. Dean[67], F. Debernardis[19,e], D. Decamp[8], V. Dedu[10], L. Del Buono[13], B. Delaney[64], H.-P. Dembinski[15], V. Denysenko[50], D. Derkach[83], O. Deschamps[9], F. Dettori[27], B. Dey[77], P. Di Nezza[23], I. Diachkov[84], S. Didenko[84], L. Dieste Maronas[46], S. Ding[68], V. Dobishuk[52], A. Dolmatov[84], C. Dong[3], A.M. Donohoe[18], F. Dordei[27], A.C. dos Reis[1], L. Douglas[59], A.G. Downes[8], P. Duda[81], M.W. Dudek[35], L. Dufour[48], V. Duk[78], P. Durante[48], M. M. Duras[81], J.M. Durham[67], D. Dutta[62], A. Dziurda[35], A. Dzyuba[38], S. Easo[57], U. Egede[69], V. Egorychev[41], C. Eirea Orro[46], S. Eisenhardt[58], E. Ejopu[62], S. Ek-In[49], L. Eklund[87], J. Ellbracht[15], S. Ely[61], A. Ene[37], E. Epple[65], S. Escher[14], J. Eschle[50], S. Esen[50], T. Evans[62], F. Fabiano[27], L.N. Falcao[1], Y. Fan[6],

B. Fang[74], L.F Fantini[78], M. Faria[49], S. Farry[60], D. Fazzini[26,l], L.F Felkowski[81], M. Féo[48], M. Fernandez Gomez[46], A.D. Fernez[66], F. Ferrari[20], L. Ferreira Lopes[49], F. Ferreira Rodrigues[2], S. Ferreres Sole[32], M. Ferrillo[50], M. Ferro-Luzzi[48], S. Filippov[39], R.A. Fini[19], M. Fiorini[21,h], M. Firlej[34], K.M. Fischer[63], D.S. Fitzgerald[88], C. Fitzpatrick[62], T. Fiutowski[34], F. Fleuret[12], M. Fontana[13], F. Fontanelli[24,j], R. Forty[48], D. Foulds-Holt[55], V. Franco Lima[60], M. Franco Sevilla[66], M. Frank[48], E. Franzoso[21,h], G. Frau[17], C. Frei[48], D.A. Friday[59], J. Fu[6], Q. Fuehring[15], T. Fulghesu[13], E. Gabriel[32], G. Galati[19,e], M.D. Galati[32], A. Gallas Torreira[46], D. Galli[20,f], S. Gambetta[58,48], M. Gandelman[2], P. Gandini[25], Y. Gao[7], Y. Gao[5], M. Garau[27], L.M. Garcia Martin[56], P. Garcia Moreno[45], J. García Pardiñas[26,l], B. Garcia Plana[46], F.A. Garcia Rosales[12], L. Garrido[45], C. Gaspar[48], R.E. Geertsema[32], D. Gerick[17], L.L. Gerken[15], E. Gersabeck[62], M. Gersabeck[62], T. Gershon[56], L. Giambastiani[28], V. Gibson[55], H.K. Giemza[36], A.L. Gilman[63], M. Giovannetti[23,r], A. Gioventù[46], P. Gironella Gironell[45], C. Giugliano[21,h], M.A. Giza[35], K. Gizdov[58], E.L. Gkougkousis[48], V.V. Gligorov[13,48], C. Göbel[70], E. Golobardes[86], D. Golubkov[41], A. Golutvin[61,84], A. Gomes[1,a], S. Gomez Fernandez[45], F. Goncalves Abrantes[63], M. Goncerz[35], G. Gong[3], I.V. Gorelov[40], C. Gotti[26], J.P. Grabowski[76], T. Grammatico[13], L.A. Granado Cardoso[48], E. Graugés[45], E. Graverini[49], G. Graziani[22], A. Grecu[37], L.M. Greeven[32], N.A. Grieser[65], L. Grillo[59], S. Gromov[84], B.R. Gruberg Cazon[63], C. Gu[3], M. Guarise[21,h], M. Guittiere[11], P. A. Günther[17], E. Gushchin[39], A. Guth[14], Y. Guz[44], T. Gys[48], T. Hadavizadeh[69], C. Hadjivasiliou[66], G. Haefeli[49], C. Haen[48], J. Haimberger[48], S.C. Haines[55], T. Halewood-leagas[60], M.M. Halvorsen[48], P.M. Hamilton[66], J.P. Hammerich[60], Q. Han[7], X. Han[17], E.B. Hansen[62], S. Hansmann-Menzemer[17], N. Harnew[63], T. Harrison[60], C. Hasse[48], M. Hatch[48], J. He[6,b], K. Heijhoff[32], F.H Hemmer[48], C. Henderson[65], R.D.L. Henderson[69,56], A.M. Hennequin[64], K. Hennessy[60], L. Henry[48], J.H Herd[61], J. Heuel[14], A. Hicheur[2], D. Hill[49], M. Hilton[62], S.E. Hollitt[15], J. Horswill[62], R. Hou[7], Y. Hou[8], J. Hu[17], J. Hu[72], W. Hu[5], X. Hu[3], W. Huang[6], X. Huang[74], W. Hulsbergen[32], R.J. Hunter[56], M. Hushchyn[83], D. Hutchcroft[60], P. Ibis[15], M. Idzik[34], D. Ilin[38], P. Ilten[65], A. Inglessi[38], A. Iniukhin[83], A. Ishteev[84], K. Ivshin[38], R. Jacobsson[48], H. Jage[14], S.J. Jaimes Elles[47], S. Jakobsen[48], E. Jans[32], B.K. Jashal[47], A. Jawahery[66], V. Jevtic[15], E. Jiang[66], X. Jiang[4], Y. Jiang[6], M. John[63], D. Johnson[64], C.R. Jones[55], T.P. Jones[56], B. Jost[48], N. Jurik[48], I. Juszczak[35], S. Kandybei[51], Y. Kang[3], M. Karacson[48], D. Karpenkov[84], M. Karpov[83], J.W. Kautz[65], F. Keizer[48], D.M. Keller[68], M. Kenzie[56], T. Ketel[32], B. Khanji[15], A. Kharisova[85], S. Kholodenko[44,84], G. Khreich[11], T. Kirn[14], V.S. Kirsebom[49], O. Kitouni[64], S. Klaver[33], N. Kleijne[29,o], K. Klimaszewski[36], M.R. Kmiec[36], S. Koliiev[52], L. Kolk[15], A. Kondybayeva[84], A. Konoplyannikov[44], P. Kopciewicz[34], R. Kopecna[17], P. Koppenburg[32], M. Korolev[40], I. Kostiuk[32,52], O. Kot[52], S. Kotriakhova[21,h], A. Kozachuk[40], P. Kravchenko[38], L. Kravchuk[39], R.D. Krawczyk[48], M. Kreps[56], S. Kretzschmar[14], P. Krokovny[43,v], W. Krupa[34], W. Krzemien[36], J. Kubat[17], S. Kubis[81], W. Kucewicz[35], M. Kucharczyk[35], V. Kudryavtsev[43,v], E.K Kulikova[42], A. Kupsc[87], D. Lacarrere[48], G. Lafferty[62,48], A. Lai[27], A. Lampis[27], D. Lancierini[50], C. Landesa Gomez[46], J.J. Lane[62], R. Lane[54], C. Langenbruch[14], J. Langer[15], O. Lantwin[84], T. Latham[56], F. Lazzari[29], M. Lazzaroni[25], R. Le Gac[10], S.H. Lee[88], R. Lefèvre[9], A. Leflat[40], S. Legotin[84], O. Leroy[10], T. Lesiak[35], B. Leverington[17], A. Li[3], H. Li[72], K. Li[7], P. Li[48], P.-R. Li[73], S. Li[7], T. Li[4], T. Li[72], Y. Li[4], Z. Li[68], X. Liang[68], C. Lin[6], T. Lin[57], R. Lindner[48], V. Lisovskyi[15], R. Litvinov[27], G. Liu[72], H. Liu[6], Q. Liu[6], S. Liu[4], A. Lobo Salvia[45], A. Loi[27], R. Lollini[78], J. Lomba Castro[46], I. Longstaff[59], J.H. Lopes[2], A. Lopez Huertas[45], S. López Soliño[46], G.H. Lovell[55], Y. Lu[4], C. Lucarelli[22,i], D. Lucchesi[28,n], S. Luchuk[39], M. Lucio Martinez[80], V. Lukashenko[32,52], Y. Luo[3], A. Lupato[62], E. Luppi[21,h], A. Lusiani[29,o], K. Lynch[18], X. Lyu[6], R. Ma[6], S. Maccolini[15], F. Machefert[11], F. Maciuc[37], I. Mackay[63], V. Macko[49], L.R. Madhan Mohan[54], O. Maev[38], A. Maevskiy[83], D. Maisuzenko[38], M.W. Majewski[34], J.J. Malczewski[35], S. Malde[63], B. Malecki[35,48], A. Malinin[82], T. Maltsev[43,v], G. Manca[27,g], G. Mancinelli[10], C. Mancuso[11,25], R. Manera Escalero[45], D. Manuzzi[20],

C.A. Manzari[50], D. Marangotto[25,k], J. Maratas[9,t], J.F. Marchand[8], U. Marconi[20], S. Mariani[22], C. Marin Benito[45], J. Marks[17], A.M. Marshall[54], P.J. Marshall[60], G. Martelli[78], G. Martellotti[30], L. Martinazzoli[48,l], M. Martinelli[26,l], D. Martinez Santos[46], F. Martinez Vidal[47], A. Massafferri[1], M. Materok[14], R. Matev[48], A. Mathad[50], V. Matiunin[41], C. Matteuzzi[26], K.R. Mattioli[12], A. Mauri[32], E. Maurice[12], J. Mauricio[45], M. Mazurek[48], M. McCann[61], L. Mcconnell[18], T.H. Mcgrath[62], N.T. Mchugh[59], A. McNab[62], R. McNulty[18], J.V. Mead[60], B. Meadows[65], G. Meier[15], D. Melnychuk[36], S. Meloni[26], M. Merk[32,80], A. Merli[25], L. Meyer Garcia[2], D. Miao[4], M. Mikhasenko[76,c], D.A. Milanes[75], E. Millard[56], M. Milovanovic[48], M.-N. Minard[8,†], A. Minotti[26,l], T. Miralles[9], S.E. Mitchell[58], B. Mitreska[15], D.S. Mitzel[15], A. Mödden [15], R.A. Mohammed[63], R.D. Moise[14], S. Mokhnenko[83], T. Mombächer[46], M. Monk[56,69], I.A. Monroy[75], S. Monteil[9], G. Morello[23], M.J. Morello[29,o], M.P. Morgenthaler[17], J. Moron[34], A.B. Morris[48], A.G. Morris[56], R. Mountain[68], H. Mu[3], E. Muhammad[56], F. Muheim[58], M. Mulder[79], K. Müller[50], C.H. Murphy[63], D. Murray[62], R. Murta[61], P. Muzzetto[27], P. Naik[54], T. Nakada[49], R. Nandakumar[57], T. Nanut[48], I. Nasteva[2], M. Needham[58], N. Neri[25,k], S. Neubert[76], N. Neufeld[48], P. Neustroev[38], R. Newcombe[61], J. Nicolini[15], D. Nicotra[80], E.M. Niel[49], S. Nieswand[14], N. Nikitin[40], N.S. Nolte[64], C. Normand[8], J. Novoa Fernandez[46], G.N Nowak[65], C. Nunez[88], A. Oblakowska-Mucha[34], V. Obraztsov[44], T. Oeser[14], D.P. O'Hanlon[54], S. Okamura[21,h], R. Oldeman[27,g], F. Oliva[58], C.J.G. Onderwater[79], R.H. O'Neil[58], J.M. Otalora Goicochea[2], T. Ovsiannikova[41], P. Owen[50], A. Oyanguren[47], O. Ozcelik[58], K.O. Padeken[76], B. Pagare[56], P.R. Pais[48], T. Pajero[63], A. Palano[19], M. Palutan[23], Y. Pan[62], G. Panshin[85], L. Paolucci[56], A. Papanestis[57], M. Pappagallo[19,e], L.L. Pappalardo[21,h], C. Pappenheimer[65], W. Parker[66], C. Parkes[62], B. Passalacqua[21,h], G. Passaleva[22], A. Pastore[19], M. Patel[61], C. Patrignani[20,f], C.J. Pawley[80], A. Pellegrino[32], M. Pepe Altarelli[48], S. Perazzini[20], D. Pereima[41], A. Pereiro Castro[46], P. Perret[9], K. Petridis[54], A. Petrolini[24,j], A. Petrov[82], S. Petrucci[58], M. Petruzzo[25,k], T.T.H. Pham[68], A. Philippov[42], R. Piandani[6], L. Pica[29,o], E. Picatoste Olloqui[45], M. Piccini[78], B. Pietrzyk[8], G. Pietrzyk[11], M. Pili[63], D. Pinci[30], F. Pisani[48], M. Pizzichemi[26,48,l], V. Placinta[37], J. Plews[53], M. Plo Casasus[46], F. Polci[13,48], M. Poli Lener[23], A. Poluektov[10], N. Polukhina[84], I. Polyakov[48], E. Polycarpo[2], S. Ponce[48], D. Popov[6,48], S. Poslavskii[44], K. Prasanth[35], L. Promberger[17], C. Prouve[46], V. Pugatch[52], V. Puill[11], G. Punzi[29,p], H. Qi[3], W. Qian[6], N. Qin[3], S. Qu[3], R. Quagliani[49], N.V. Raab[18], B. Rachwal[34], J.H. Rademacker[54], R. Rajagopalan[68], M. Rama[29,p], M. Ramos Pernas[56], M.S. Rangel[2], F. Ratnikov[42,83], G. Raven[33,48], M. Rebollo De Miguel[47], F. Redi[48], J. Reich[54], F. Reiss[62], C. Remon Alepuz[47], Z. Ren[3], P.K. Resmi[10], R. Ribatti[29,o], A.M. Ricci[27], S. Ricciardi[57], K. Richardson[64], M. Richardson-Slipper[58], K. Rinnert[60], P. Robbe[11], G. Robertson[58], A.B. Rodrigues[49], E. Rodrigues[60], E. Rodriguez Fernandez[46], J.A. Rodriguez Lopez[75], E.R.R. Rodriguez Rodriguez[46], D.L. Rolf[48], A. Rollings[63], P. Roloff[48], V. Romanovskiy[44], M. Romero Lamas[46], A. Romero Vidal[46], M. Rosello[86], J.D. Roth[88,†], M. Rotondo[23], M.S. Rudolph[68], T. Ruf[48], R.A. Ruiz Fernandez[46], J. Ruiz Vidal[47], A. Ryzhikov[83], J. Ryzka[34], J.J. Saborido Silva[46], N. Sagidova[38], N. Sahoo[53], B. Saitta[27,g], M. Salomoni[48], C. Sanchez Gras[32], I. Sanderswood[47], R. Santacesaria[30], C. Santamarina Rios[46], M. Santimaria[23], E. Santovetti[31,r], D. Saranin[84], G. Sarpis[14], M. Sarpis[76], A. Sarti[30], C. Satriano[30,q], A. Satta[31], M. Saur[15], D. Savrina[40,41], H. Sazak[9], L.G. Scantlebury Smead[63], A. Scarabotto[13], S. Schael[14], S. Scherl[60], M. Schiller[59], H. Schindler[48], M. Schmelling[16], B. Schmidt[48], S. Schmitt[14], O. Schneider[49], A. Schopper[48], M. Schubiger[32], S. Schulte[49], M.H. Schune[11], R. Schwemmer[48], B. Sciascia[23], A. Sciuccati[48], S. Sellam[46], A. Semennikov[41], M. Senghi Soares[33], A. Sergi[24,j], N. Serra[50], L. Sestini[28], A. Seuthe[15], Y. Shang[5], D.M. Shangase[88], M. Shapkin[44], I. Shchemerov[84], L. Shchutska[49], T. Shears[60], L. Shekhtman[43,v], Z. Shen[5], S. Sheng[4], V. Shevchenko[82], B. Shi[6], E.B. Shields[26,l], Y. Shimizu[11], E. Shmanin[84], R. Shorkin[84], J.D. Shupperd[68], B.G. Siddi[21], R. Silva Coutinho[68], G. Simi[28], S. Simone[19,e], M. Singla[69], N. Skidmore[62], R. Skuza[17], T. Skwarnicki[68], M.W. Slater[53],

J.C. Smallwood[63], J.G. Smeaton[55], E. Smith[50], K. Smith[67], M. Smith[61], A. Snoch[32], L. Soares Lavra[9], M.D. Sokoloff[65], F.J.P. Soler[59], A. Solomin[40,54], A. Solovev[38], I. Solovyev[38], R. Song[69], F.L. Souza De Almeida[2], B. Souza De Paula[2], B. Spaan[15,†], E. Spadaro Norella[25,k], E. Spedicato[20], E. Spiridenkov[38], P. Spradlin[59], V. Sriskaran[48], F. Stagni[48], M. Stahl[48], S. Stahl[48], S. Stanislaus[63], E.N. Stein[48], O. Steinkamp[50], O. Stenyakin[44], H. Stevens[15], S. Stone[68,48,†], D. Strekalina[84], Y.S Su[6], F. Suljik[63], J. Sun[27], L. Sun[74], Y. Sun[66], P. Svihra[62], P.N. Swallow[53], K. Swientek[34], A. Szabelski[36], T. Szumlak[34], M. Szymanski[48], Y. Tan[3], S. Taneja[62], M.D. Tat[63], A. Terentev[84], F. Teubert[48], E. Thomas[48], D.J.D. Thompson[53], K.A. Thomson[60], H. Tilquin[61], V. Tisserand[9], S. T'Jampens[8], M. Tobin[4], L. Tomassetti[21,h], G. Tonani[25], X. Tong[5], D. Torres Machado[1], D.Y. Tou[3], S.M. Trilov[54], C. Trippl[49], G. Tuci[6], N. Tuning[32], A. Ukleja[36], D.J. Unverzagt[17], A. Usachov[32], A. Ustyuzhanin[42,83], U. Uwer[17], A. Vagner[85], V. Vagnoni[20], A. Valassi[48], G. Valenti[20], N. Valls Canudas[86], M. Van Dijk[48], H. Van Hecke[67], E. van Herwijnen[61], C.B. Van Hulse[46,w], M. van Veghel[32], R. Vazquez Gomez[45], P. Vazquez Regueiro[46], C. Vázquez Sierra[48], S. Vecchi[21], J.J. Velthuis[54], M. Veltri[22,s], A. Venkateswaran[49], M. Veronesi[32], M. Vesterinen[56], D. Vieira[65], M. Vieites Diaz[49], X. Vilasis-Cardona[86], E. Vilella Figueras[60], A. Villa[20], P. Vincent[13], F.C. Volle[11], D. Vom Bruch[10], A. Vorobyev[38], V. Vorobyev[43], N. Voropaev[38], K. Vos[80], C. Vrahas[58], J. Walsh[29,p], G. Wan[5], C. Wang[17], G. Wang[7], J. Wang[5], J. Wang[4], J. Wang[3], J. Wang[74], M. Wang[25], R. Wang[54], X. Wang[72], Y. Wang[7], Z. Wang[50], Z. Wang[3], Z. Wang[6], J.A. Ward[56,69], N.K. Watson[53], D. Websdale[61], Y. Wei[5], B.D.C. Westhenry[54], D.J. White[62], M. Whitehead[59], A.R. Wiederhold[56], D. Wiedner[15], G. Wilkinson[63], M. K. Wilkinson[65], I. Williams[55], M. Williams[64], M.R.J. Williams[58], R. Williams[55], F.F. Wilson[57], W. Wislicki[36], M. Witek[35], L. Witola[17], C.P. Wong[67], G. Wormser[11], S.A. Wotton[55], H. Wu[68], J. Wu[7], K. Wyllie[48], Z. Xiang[6], Y. Xie[7], A. Xu[5], J. Xu[6], L. Xu[3], L. Xu[3], M. Xu[56], Q. Xu[6], Z. Xu[9], Z. Xu[6], D. Yang[3], S. Yang[6], X. Yang[5], Y. Yang[6], Z. Yang[5], Z. Yang[66], L.E. Yeomans[60], V. Yeroshenko[11], H. Yeung[62], H. Yin[7], J. Yu[71], X. Yuan[68], O. Yushchenko[44], E. Zaffaroni[49], M. Zavertyaev[16,u], M. Zdybal[35], M. Zeng[3], C. Zhang[5], D. Zhang[7], L. Zhang[3], S. Zhang[71], S. Zhang[5], Y. Zhang[5], Y. Zhang[63], Y. Zhao[17], A. Zharkova[84], A. Zhelezov[17], Y. Zheng[6], T. Zhou[5], X. Zhou[6], Y. Zhou[6], V. Zhovkovska[11], X. Zhu[3], X. Zhu[7], Z. Zhu[6], V. Zhukov[14,40], Q. Zou[4], S. Zucchelli[20,f], D. Zuliani[28], G. Zunica[62].

[1] *Centro Brasileiro de Pesquisas Físicas (CBPF), Rio de Janeiro, Brazil*
[2] *Universidade Federal do Rio de Janeiro (UFRJ), Rio de Janeiro, Brazil*
[3] *Center for High Energy Physics, Tsinghua University, Beijing, China*
[4] *Institute Of High Energy Physics (IHEP), Beijing, China*
[5] *School of Physics State Key Laboratory of Nuclear Physics and Technology, Peking University, Beijing, China*
[6] *University of Chinese Academy of Sciences, Beijing, China*
[7] *Institute of Particle Physics, Central China Normal University, Wuhan, Hubei, China*
[8] *Université Savoie Mont Blanc, CNRS, IN2P3-LAPP, Annecy, France*
[9] *Université Clermont Auvergne, CNRS/IN2P3, LPC, Clermont-Ferrand, France*
[10] *Aix Marseille Univ, CNRS/IN2P3, CPPM, Marseille, France*
[11] *Université Paris-Saclay, CNRS/IN2P3, IJCLab, Orsay, France*
[12] *Laboratoire Leprince-Ringuet, CNRS/IN2P3, Ecole Polytechnique, Institut Polytechnique de Paris, Palaiseau, France*
[13] *LPNHE, Sorbonne Université, Paris Diderot Sorbonne Paris Cité, CNRS/IN2P3, Paris, France*
[14] *I. Physikalisches Institut, RWTH Aachen University, Aachen, Germany*
[15] *Fakultät Physik, Technische Universität Dortmund, Dortmund, Germany*
[16] *Max-Planck-Institut für Kernphysik (MPIK), Heidelberg, Germany*
[17] *Physikalisches Institut, Ruprecht-Karls-Universität Heidelberg, Heidelberg, Germany*
[18] *School of Physics, University College Dublin, Dublin, Ireland*
[19] *INFN Sezione di Bari, Bari, Italy*
[20] *INFN Sezione di Bologna, Bologna, Italy*

[21] *INFN Sezione di Ferrara, Ferrara, Italy*
[22] *INFN Sezione di Firenze, Firenze, Italy*
[23] *INFN Laboratori Nazionali di Frascati, Frascati, Italy*
[24] *INFN Sezione di Genova, Genova, Italy*
[25] *INFN Sezione di Milano, Milano, Italy*
[26] *INFN Sezione di Milano-Bicocca, Milano, Italy*
[27] *INFN Sezione di Cagliari, Monserrato, Italy*
[28] *Universita degli Studi di Padova, Universita e INFN, Padova, Padova, Italy*
[29] *INFN Sezione di Pisa, Pisa, Italy*
[30] *INFN Sezione di Roma La Sapienza, Roma, Italy*
[31] *INFN Sezione di Roma Tor Vergata, Roma, Italy*
[32] *Nikhef National Institute for Subatomic Physics, Amsterdam, Netherlands*
[33] *Nikhef National Institute for Subatomic Physics and VU University Amsterdam, Amsterdam, Netherlands*
[34] *AGH - University of Science and Technology, Faculty of Physics and Applied Computer Science, Kraków, Poland*
[35] *Henryk Niewodniczanski Institute of Nuclear Physics Polish Academy of Sciences, Kraków, Poland*
[36] *National Center for Nuclear Research (NCBJ), Warsaw, Poland*
[37] *Horia Hulubei National Institute of Physics and Nuclear Engineering, Bucharest-Magurele, Romania*
[38] *Petersburg Nuclear Physics Institute NRC Kurchatov Institute (PNPI NRC KI), Gatchina, Russia*
[39] *Institute for Nuclear Research of the Russian Academy of Sciences (INR RAS), Moscow, Russia*
[40] *Institute of Nuclear Physics, Moscow State University (SINP MSU), Moscow, Russia*
[41] *Institute of Theoretical and Experimental Physics NRC Kurchatov Institute (ITEP NRC KI), Moscow, Russia*
[42] *Yandex School of Data Analysis, Moscow, Russia*
[43] *Budker Institute of Nuclear Physics (SB RAS), Novosibirsk, Russia*
[44] *Institute for High Energy Physics NRC Kurchatov Institute (IHEP NRC KI), Protvino, Russia, Protvino, Russia*
[45] *ICCUB, Universitat de Barcelona, Barcelona, Spain*
[46] *Instituto Galego de Física de Altas Enerxías (IGFAE), Universidade de Santiago de Compostela, Santiago de Compostela, Spain*
[47] *Instituto de Fisica Corpuscular, Centro Mixto Universidad de Valencia - CSIC, Valencia, Spain*
[48] *European Organization for Nuclear Research (CERN), Geneva, Switzerland*
[49] *Institute of Physics, Ecole Polytechnique Fédérale de Lausanne (EPFL), Lausanne, Switzerland*
[50] *Physik-Institut, Universität Zürich, Zürich, Switzerland*
[51] *NSC Kharkiv Institute of Physics and Technology (NSC KIPT), Kharkiv, Ukraine*
[52] *Institute for Nuclear Research of the National Academy of Sciences (KINR), Kyiv, Ukraine*
[53] *University of Birmingham, Birmingham, United Kingdom*
[54] *H.H. Wills Physics Laboratory, University of Bristol, Bristol, United Kingdom*
[55] *Cavendish Laboratory, University of Cambridge, Cambridge, United Kingdom*
[56] *Department of Physics, University of Warwick, Coventry, United Kingdom*
[57] *STFC Rutherford Appleton Laboratory, Didcot, United Kingdom*
[58] *School of Physics and Astronomy, University of Edinburgh, Edinburgh, United Kingdom*
[59] *School of Physics and Astronomy, University of Glasgow, Glasgow, United Kingdom*
[60] *Oliver Lodge Laboratory, University of Liverpool, Liverpool, United Kingdom*
[61] *Imperial College London, London, United Kingdom*
[62] *Department of Physics and Astronomy, University of Manchester, Manchester, United Kingdom*
[63] *Department of Physics, University of Oxford, Oxford, United Kingdom*
[64] *Massachusetts Institute of Technology, Cambridge, MA, United States*
[65] *University of Cincinnati, Cincinnati, OH, United States*
[66] *University of Maryland, College Park, MD, United States*
[67] *Los Alamos National Laboratory (LANL), Los Alamos, NM, United States*
[68] *Syracuse University, Syracuse, NY, United States*
[69] *School of Physics and Astronomy, Monash University, Melbourne, Australia, associated to* [56]
[70] *Pontifícia Universidade Católica do Rio de Janeiro (PUC-Rio), Rio de Janeiro, Brazil, associated to* [2]
[71] *Physics and Micro Electronic College, Hunan University, Changsha City, China, associated to* [7]

[72] *Guangdong Provincial Key Laboratory of Nuclear Science, Guangdong-Hong Kong Joint Laboratory of Quantum Matter, Institute of Quantum Matter, South China Normal University, Guangzhou, China, associated to* [3]
[73] *Lanzhou University, Lanzhou, China, associated to* [4]
[74] *School of Physics and Technology, Wuhan University, Wuhan, China, associated to* [3]
[75] *Departamento de Fisica , Universidad Nacional de Colombia, Bogota, Colombia, associated to* [13]
[76] *Universität Bonn - Helmholtz-Institut für Strahlen und Kernphysik, Bonn, Germany, associated to* [17]
[77] *Eotvos Lorand University, Budapest, Hungary, associated to* [48]
[78] *INFN Sezione di Perugia, Perugia, Italy, associated to* [21]
[79] *Van Swinderen Institute, University of Groningen, Groningen, Netherlands, associated to* [32]
[80] *Universiteit Maastricht, Maastricht, Netherlands, associated to* [32]
[81] *Faculty of Material Engineering and Physics, Cracow, Poland, associated to* [35]
[82] *National Research Centre Kurchatov Institute, Moscow, Russia, associated to* [41]
[83] *National Research University Higher School of Economics, Moscow, Russia, associated to* [42]
[84] *National University of Science and Technology "MISIS", Moscow, Russia, associated to* [41]
[85] *National Research Tomsk Polytechnic University, Tomsk, Russia, associated to* [41]
[86] *DS4DS, La Salle, Universitat Ramon Llull, Barcelona, Spain, associated to* [45]
[87] *Department of Physics and Astronomy, Uppsala University, Uppsala, Sweden, associated to* [59]
[88] *University of Michigan, Ann Arbor, MI, United States, associated to* [68]

[a] *Universidade de Brasília, Brasília, Brazil*
[b] *Hangzhou Institute for Advanced Study, UCAS, Hangzhou, China*
[c] *Excellence Cluster ORIGINS, Munich, Germany*
[d] *Universidad Nacional Autonoma de Honduras, Tegucigalpa, Honduras*
[e] *Università di Bari, Bari, Italy*
[f] *Università di Bologna, Bologna, Italy*
[g] *Università di Cagliari, Cagliari, Italy*
[h] *Università di Ferrara, Ferrara, Italy*
[i] *Università di Firenze, Firenze, Italy*
[j] *Università di Genova, Genova, Italy*
[k] *Università degli Studi di Milano, Milano, Italy*
[l] *Università di Milano Bicocca, Milano, Italy*
[m] *Università di Modena e Reggio Emilia, Modena, Italy*
[n] *Università di Padova, Padova, Italy*
[o] *Scuola Normale Superiore, Pisa, Italy*
[p] *Università di Pisa, Pisa, Italy*
[q] *Università della Basilicata, Potenza, Italy*
[r] *Università di Roma Tor Vergata, Roma, Italy*
[s] *Università di Urbino, Urbino, Italy*
[t] *MSU - Iligan Institute of Technology (MSU-IIT), Iligan, Philippines*
[u] *P.N. Lebedev Physical Institute, Russian Academy of Science (LPI RAS), Moscow, Russia*
[v] *Novosibirsk State University, Novosibirsk, Russia*
[w] *Universidad de Alcalá, Alcalá de Henares , Spain*

[†] *Deceased*